CLASSIFICATION CANCELLED

~~RESTRICTED~~

COPY No. 5
RM No. E8H13

NACA form 473 12-12-58

By M H Dilts

1-23-51

Copy 2

NACA RM No. E8H13

RESEARCH MEMORANDUM

PERFORMANCE INVESTIGATIONS OF A LARGE CENTRIFUGAL COMPRESSOR FROM AN EXPERIMENTAL TURBOJET ENGINE

By Ambrose Ginsburg, John W. R. Creagh
and William K. Ritter

Lewis Flight Propulsion Laboratory
Cleveland, Ohio

CLASSIFIED DOCUMENT

This document contains classified information affecting the National Defense of the United States within the meaning of the Espionage Act, USC 50:31 and 32. Its transmission or the revelation of its contents in any manner to an unauthorized person is prohibited by law. Information so classified may be imparted only to persons in the military and naval services of the United States, appropriate civilian officers and employees of the Federal Government who have a legitimate interest therein, and to United States citizens of known loyalty and discretion who of necessity must be informed thereof.

NATIONAL ADVISORY COMMITTEE
FOR AERONAUTICS

WASHINGTON
October 18, 1948

~~RESTRICTED~~

N A C A LIBRARY
LANGLEY MEMORIAL AERONAUTICAL
LABORATORY

NASA Technical Library
3 1176 01435 5524

NATIONAL ADVISORY COMMITTEE FOR AERONAUTICS

RESEARCH MEMORANDUM

PERFORMANCE INVESTIGATIONS OF A LARGE CENTRIFUGAL COMPRESSOR FROM AN EXPERIMENTAL TURBOJET ENGINE

By Ambrose Ginsburg, John W. R. Creagh
and William K. Ritter

SUMMARY

An investigation was conducted on a large centrifugal compressor from an experimental turbojet engine to determine the performance of the compressor and to obtain fundamental information on the aerodynamic problems associated with large centrifugal-type compressors.

The results of the research conducted on the compressor indicated that the compressor would not meet the desired engine-design air-flow requirements (78 lb/sec) because of an air-flow restriction in the vaned collector (diffuser). Revision of the vaned collector resulted in an increased air-flow capacity over the speed range and showed improved matching of the impeller and diffuser components.

At maximum flow, the original compressor utilized approximately 90 percent of the available geometric throat area at the vaned-collector inlet and the revised compressor utilized approximately 94 percent, regardless of impeller speed. The ratio of the maximum weight flows of the revised and original compressors was less than the ratio of effective critical throat areas of the two compressors because of large pressure losses in the impeller near the impeller inlet and the difference increased with an increase in impeller speed. In order to further increase the pressure ratio and maximum weight flow of the compressor, the impeller must be modified to eliminate the pressure losses therein.

INTRODUCTION

The compressor is one of the most important elements of the aircraft turbine-type engine. The centrifugal compressor, upon which Whittle of England developed the first practical turbojet engine for aircraft propulsion, has several favorable characteristics such as dependability, simplicity, and ease of manufacture. Considerable work has been done in the past to improve the performance of the small centrifugal compressor as a highly useful accessory of the reciprocating engine, but because of the much larger air capacity and power requirements of the turbojet-engine compressor as well as its newness, very little information on the performance of compressors of this type has been published.

An investigation covering the performance characteristics and air-flow analysis of a centrifugal compressor used in an experimental turbojet engine was conducted at the NACA Cleveland laboratory. The impeller was a single-entry type and had an inlet-to-outlet diameter ratio of 0.65, which resulted in transonic Mach numbers near the inlet-blade tip at design conditions. The diffuser had unusual design features in that the air-flow path through the diffuser had an increasing and then a decreasing radius of rotation. For this investigation, extensive instrumentation was used along an air-flow path through the compressor; from this instrumentation, the determination of the over-all compressor performance and the analysis of the performance of the component parts of the compressor were possible. As a result of the analysis of the compressor performance, a modification was recommended to obtain improved performance. The recommended changes were made in a second compressor, which, in turn, was similarly investigated. The investigation of the second compressor was extended to cover a brief survey of the effects on performance of changing the inlet-air pressure and temperature.

APPARATUS

Two turbojet-engine compressors were investigated. The first compressor, hereinafter called the original compressor, consisted of a single-entry centrifugal impeller, a vaneless diffuser followed by a vaned collector, and accessory shrouds and casings. The compressor had a rated air-flow capacity of 78 pounds per second at a pressure ratio of 4.0 and an equivalent impeller speed of 11,500 rpm. Front and rear views of the original-compressor assembly are presented in figure 1. The impeller had a blade-tip diameter of 20.75 inches at the inlet, a blade-tip diameter of 32.00 inches at the outlet, 18 full blades, and 18 splitter blades. The maximum over-all diameter of the compressor was approximately 48 inches. A view of the original compressor with the front cover removed is shown in figure 2. The general nature of the impeller-blade construction, the relative magnitude of the vaneless-diffuser section, and the inlet portion of the vaned collector can be seen in the figure. The flow path through the vaned collector had an increasing and then a decreasing radius of rotation. The vaned collector was designed to have no radial component of flow at the inlet to the burner annulus.

The research investigation of the original compressor was terminated by a structural failure of the compressor in attempting to run at rated speed. As a result of the manufacturer's investigation of the accident, the impeller blades were found to have evidently suffered a fatigue failure due to the presence, at speeds near the design value, of resonant exciting frequencies from the field of aerodynamic force created by the three equally spaced inlet cover struts.

From this failure and the analysis of the compressor-performance data, a second compressor was constructed in an attempt to reach design speed and to improve the compressor performance at all speeds. A view of this second compressor, hereinafter called the revised compressor, with the front cover removed is shown in figure 3. Two important changes were made to the original compressor:

1. The impeller blades were slightly altered to increase their natural frequency by machining a small amount of metal from the corner of each blade at the leading edge and by increasing the blade taper near the leading edge.

2. The vaned-collector inlet was modified to improve the air-flow performance of the compressor by cutting back the inlet edges of the vanes. With the exception of these changes, the original and revised compressors were otherwise essentially the same.

The compressor test installation is shown in figure 4. The collecting chamber on which each of the compressors was mounted contained an annular section, which simulated the burner section of the turbojet engine. The collecting chamber was designed to maintain uniform flow in the simulated burner annulus and care was taken to avoid possible limitation of compressor-flow capacity by choking in the chamber. The compressor was driven by a 6000-horsepower variable-speed electric motor in conjunction with a speed-increaser gear. The inlet pipe was 24 inches in diameter and 12 diameters long; the discharge pipe was 16 inches in diameter and 5 diameters long and was preceded by a transition section approximately 3 feet long. No insulation material was used on the compressor, the collecting chamber or the inlet and the outlet pipes.

INSTRUMENTATION

The original compressor was extensively instrumented to determine the over-all performance of the compressor and the characteristic performance of each of the compressor components. Eighty-four static-pressure taps were installed to determine the performance of the impeller and the diffuser. The compressor instrumentation is shown in figure 5. Most of the outer-wall static-pressure taps are shown as well as the bulkhead and fittings used to facilitate connection of the inner-wall static-pressure taps to manometers. A complete listing of the static-pressure station locations is given in table I using the number designations shown in figure 5. It can be seen from the table that with the exception of the pressure taps 1 through 12(b) along the front cover and 28 in the simulated burner annulus, every tap on the outer wall was accompanied by a corresponding inner-wall tap located in such a manner that a line joining the two would be approximately perpendicular to the air stream at that section. A schematic diagram of a typical flow path through the original compressor is shown in figure 6 together with the number designations of the pertinent static-pressure stations. Also shown is the simulated burner annulus section into which the compressor discharged.

The instrumentation on the revised compressor was less extensive than on the original compressor because as a result of the performance investigation of the original compressor, some static taps could be eliminated because of the similarity of flow conditions. From table I, the total number of static-pressure taps was reduced from 84 on the original compressor to 42 on the revised compressor. Despite the reduction in the number of static-pressure taps, the instrumentation along a flow path was maintained as shown in figure 6 except that static-pressure tap 27 was eliminated in the vaned-collector passage.

Standard instrumentation was installed in the inlet pipe according to the methods described in references 1 and 2. The simulated burner annulus was equipped with 10 total-pressure, 5 static-pressure, and 10 temperature-measuring stations to determine the air-stream conditions at the compressor outlet. A remotely controlled survey probe of the Fechheimer type (reference 3) was provided to measure the angularity of the air stream and the total-pressure gradient of the air entering a typical vaned-collector passage. This probe was installed normal to the air-flow passage walls and approximately 1 inch ahead of the center of the inlet to a vaned-collector passage; the distance was measured along the mean flow-path line. Air-flow and pressure regulation were provided by butterfly-type throttle valves installed in the inlet and the outlet pipes. An adjustable submerged orifice measured the quantity of air flow. Mercury manometers were used to measure all pressures except the differential pressure across the air-metering orifice, which was measured with a water manometer. A chronometric tachometer was used to provide accurate indication of the impeller speed. A calibrated potentiometer with a sensitive light-beam galvanometer was used to measure the temperature of the air stream.

PROCEDURE

Original Compressor

The compressor was run at equivalent impeller speeds of 5000, 7000, 8000, 9000, and 10,000 rpm. A complete failure of the compressor prevented obtaining data above the equivalent speed of 10,000 rpm. All of the runs were made with ambient inlet-air temperature and an inlet-air stagnation pressure of approximately 14 inches of mercury absolute, except for the low compressor pressure ratios at maximum flow for which higher inlet-air pressures were used. Inlet-air pressures of 14 inches of mercury absolute were used in order that the complete range of compressor speeds might be investigated at the same inlet-air-pressure conditions with a 6000-horsepower driving motor. Surveys of the air stream were made at the inlet to the vaned collector at equivalent impeller speeds of 5000, 7000, 8000, and 9000 rpm.

Revised Compressor

This compressor was operated under the following conditions:

Equivalent speed (rpm)	Inlet		Outlet
	Total pressure (in. Hg abs.)	Temperature	Total pressure (in. Hg abs.)
3,600	- - -	Ambient	31
5,000	- - -	Ambient	33
7,000	14	Ambient	- - -
8,000	14	Ambient	- - -
8,000	8	-32° F	- - -
8,000	8	Ambient	- - -
9,000	14	Ambient	- - -
10,000	14	Ambient	- - -
11,200	14	Ambient	- - -
11,500	6	-32° F	- - -

Low inlet-air total pressures were not used at equivalent impeller speeds of 3600 and 5000 rpm because of possible adverse pressure differentials on the impeller casing at these speeds. At the manufacturer's request, an actual impeller speed of 11,500 rpm was set as the maximum allowable speed for this investigation. Inasmuch as no means were available at the time for regulating the inlet-air temperature between the ambient value of approximately 80° F and the laboratory refrigerated-air value of approximately -32° F, one run was made at maximum allowable speed with ambient inlet air and another at an equivalent speed of 11,500 rpm with an inlet-air temperature of -32° F. Only one point (maximum flow) was taken at maximum impeller speed under ambient-temperature conditions and the resulting equivalent speed was 11,200 rpm. Because of mass-flow limitations of the refrigerated-air supply, the inlet-air pressure had to be reduced to 6 inches of mercury absolute when a temperature of -32° F was used. The equivalent speed of 8000 rpm was investigated at three inlet conditions to correlate the effects of inlet conditions on the compressor performance.

RATING METHODS

Compressor

The performance of the compressor was based on the measured total pressures and temperatures at the impeller inlet and at the outlet of the simulated burner annulus. Computations of adiabatic efficiency η_{ad} for the compressor were made in accordance with reference 1. The flow parameter, corrected weight flow $W\sqrt{\theta}/\delta$, and the speed parameter, equivalent impeller speed $N/\sqrt{\theta}$, were computed according to the method of reference 4, where

W air weight flow at inlet conditions, (lb/sec)

θ ratio of actual inlet stagnation absolute temperature to standard sea-level absolute temperature

δ ratio of actual inlet stagnation pressure to standard sea-level pressure

N actual impeller speed, (rpm)

(All symbols are defined in the text when first used. A symbol list is given in appendix A.)

Impeller

The impeller performance was determined for each speed from measurements in the vaneless-diffuser passage 1/8 inch from the

966

PROCEDURE

Original Compressor

The compressor was run at equivalent impeller speeds of 5000, 7000, 8000, 9000, and 10,000 rpm. A complete failure of the compressor prevented obtaining data above the equivalent speed of 10,000 rpm. All of the runs were made with ambient inlet-air temperature and an inlet-air stagnation pressure of approximately 14 inches of mercury absolute, except for the low compressor pressure ratios at maximum flow for which higher inlet-air pressures were used. Inlet-air pressures of 14 inches of mercury absolute were used in order that the complete range of compressor speeds might be investigated at the same inlet-air-pressure conditions with a 6000-horsepower driving motor. Surveys of the air stream were made at the inlet to the vaned collector at equivalent impeller speeds of 5000, 7000, 8000, and 9000 rpm.

Revised Compressor

This compressor was operated under the following conditions:

Equivalent speed (rpm)	Inlet		Outlet
	Total pressure (in. Hg abs.)	Temperature	Total pressure (in. Hg abs.)
3,600	- - -	Ambient	31
5,000	- - -	Ambient	33
7,000	14	Ambient	- - -
8,000	14	Ambient	- - -
8,000	8	-32° F	- - -
8,000	8	Ambient	- - -
9,000	14	Ambient	- - -
10,000	14	Ambient	- - -
11,200	14	Ambient	- - -
11,500	6	-32° F	- - -

Low inlet-air total pressures were not used at equivalent impeller speeds of 3600 and 5000 rpm because of possible adverse pressure differentials on the impeller casing at these speeds. At the manufacturer's request, an actual impeller speed of 11,500 rpm was set as the maximum allowable speed for this investigation. Inasmuch as no means were available at the time for regulating the inlet-air temperature between the ambient value of approximately 80° F and the laboratory refrigerated-air value of approximately -32° F, one run was made at maximum allowable speed with ambient inlet air and another at an equivalent speed of 11,500 rpm with an inlet-air temperature of -32° F. Only one point (maximum flow) was taken at maximum impeller speed under ambient-temperature conditions and the resulting equivalent speed was 11,200 rpm. Because of mass-flow limitations of the refrigerated-air supply, the inlet-air pressure had to be reduced to 6 inches of mercury absolute when a temperature of -32° F was used. The equivalent speed of 8000 rpm was investigated at three inlet conditions to correlate the effects of inlet conditions on the compressor performance.

RATING METHODS

Compressor

The performance of the compressor was based on the measured total pressures and temperatures at the impeller inlet and at the outlet of the simulated burner annulus. Computations of adiabatic efficiency η_{ad} for the compressor were made in accordance with reference 1. The flow parameter, corrected weight flow $W\sqrt{\theta}/\delta$, and the speed parameter, equivalent impeller speed $N/\sqrt{\theta}$, were computed according to the method of reference 4, where

W air weight flow at inlet conditions, (lb/sec)

θ ratio of actual inlet stagnation absolute temperature to standard sea-level absolute temperature

δ ratio of actual inlet stagnation pressure to standard sea-level pressure

N actual impeller speed, (rpm)

(All symbols are defined in the text when first used. A symbol list is given in appendix A.)

Impeller

The impeller performance was determined for each speed from measurements in the vaneless-diffuser passage 1/8 inch from the impeller-outlet blade tip. The total pressure was determined from the computed dynamic pressure and the measured static pressure. The calculations were made on the assumption that there was no change in total temperature of the air from the impeller tip through the system to the measuring stations in the simulated burner annulus, that the friction loss between the impeller outlet and the measuring point was negligible, and that the velocity was constant across the diffuser passage. The air velocity and the density were determined from the measured static pressure, the continuity of flow, and the foregoing assumptions. Computations of adiabatic efficiency for the impeller were made in accordance with reference 1.

Diffuser

The vaneless diffuser and the vaned collector were rated together as a diffuser. Diffuser efficiency was defined as the ratio of the actual static-pressure rise between the impeller outlet and the simulated burner annulus to the isentropic static-pressure rise theoretically obtained from the change in Mach numbers between the same two points. The following form of Bernoulli's equation for a gas was used to obtain the efficiency equation

$$\frac{P}{p} = \left[1 + \left(\frac{\gamma-1}{2}\right) M^2\right]^{\frac{\gamma}{\gamma-1}} \qquad (1)$$

where

P stagnation pressure, (in. Hg absolute)

p static pressure, (in. Hg absolute)

γ ratio of specific heats

M Mach number

Values of Mach number were determined from the measured total temperatures and the static temperatures calculated at the impeller outlet and in the simulated burner annulus. Inasmuch as the process is isentropic and there is no change in stagnation pressure, if subscripts 1 and 4 are used to refer to stations at the impeller outlet and the simulated burner annulus, respectively, the following equation may be written:

$$\frac{\left(\frac{P}{p}\right)_1}{\left(\frac{P}{p}\right)_4} = \left[\frac{2 + (\gamma-1)\ M_1^{\ 2}}{2 + (\gamma-1)\ M_4^{\ 2}}\right]^{\frac{\gamma}{\gamma-1}} = \frac{p_4}{p_1}$$

which is the ideal or reversible static-pressure ratio. If the actual static-pressure ratio between the same two points is denoted by Q then, inasmuch as the diffuser is rated on a pressure-rise basis and pressure ratios less than 1.0 are not pertinent, the diffuser efficiency is expressed as

$$\text{diffuser efficiency} = \frac{Q - 1}{\left[\frac{2 + (\gamma-1)\ M_1^{\ 2}}{2 + (\gamma-1)\ M_4^{\ 2}}\right]^{\frac{\gamma}{\gamma-1}} - 1}$$

RESULTS AND DISCUSSION

Original Compressor

Compressor performance. - The compressor performance characteristics over the range of compressor (equivalent impeller) speeds from 5000 to 10,000 rpm are shown in figure 7. A peak adiabatic efficiency η_{ad} of 0.80 was obtained at an equivalent impeller speed of 9000 rpm, and a corrected weight flow of 47 pounds per second, and a pressure ratio of 2.60. The maximum pressure ratio was 3.17 and occurred at an equivalent impeller speed of 10,000 rpm, a corrected weight flow of 49 pounds per second, and an adiabatic efficiency of approximately 0.77. As shown on figure 7, the maximum corrected weight flow at an equivalent impeller speed of 10,000 rpm was 63 pounds per second.

The compressor weight-flow variation with equivalent impeller speed for maximum flow and for selected compressor efficiencies is shown in figure 8. The curves represent peak adiabatic efficiency, constant adiabatic efficiencies of 0.70 and, 0.75 and maximum corrected weight flow. The turbojet engine weight-flow design point of 78 pounds per second at rated speed of 11,500 rpm is also shown. Extrapolation of the maximum-weight-flow or choking-flow line to rated speed indicates that the maximum weight flow obtainable at rated speed will probably be below the engine design requirement. Inasmuch as the 0.70 and 0.75

efficiency lines, which approximate the engine operating range, lie below the maximum-flow curve, the compressor would probably not have met the required performance for the design engine operating conditions.

Compressor-component performance. - The impeller, compressor, and diffuser efficiencies are shown in figure 9.

The impeller-efficiency curves have a generally flat characteristic over the weight-flow range with peak efficiency at or near maximum compressor weight flow. The maximum calculated efficiency, 0.93, occurred at a speed of 5000 rpm. The drop in impeller efficiency with increasing speed was small; the peak efficiency at an equivalent speed of 10,000 rpm was 0.89. The comparatively small variation in the impeller-efficiency curves indicates that the compressor-flow restriction or choking point does not occur in the impeller, because choking in the impeller would result in pressure losses and a sharp drop in the impeller efficiency at the maximum-flow points. The values of impeller efficiencies indicate that this component has good performance characteristics.

The values of diffuser efficiencies are considerably lower than the impeller efficiencies; a maximum value of 0.74 was obtained at 9000 rpm. In addition, the diffuser curves are quite peaked and, as the peaks of the impeller and diffuser curves do not coincide because of imperfect matching of these components, the over-all performance of the compressor was adversely affected. Of more importance, however, is the rapidity with which the diffuser efficiency falls off at the high air flows, which indicates that pressure losses accompanying choking occurred somewhere in the diffuser.

Flow capacity and limitations. - Static-pressure ratios (local static pressure/impeller-inlet static pressure) at three stations around the periphery of the inner and outer walls of the vaned-collector inlet are shown in figure 10 at an equivalent impeller speed of 8000 rpm. The static-pressure ratios at the outlet of each vaned-collector passage on the inner and outer walls are shown at an equivalent impeller speed of 8000 rpm in figure 11. These curves indicate that the flow was very nearly uniform around the periphery of the compressor and that measurements taken in one vaned-collector passage or at one set of radial stations in the vaneless diffuser should therefore be typical of measurements taken at any other position around the periphery.

The static-pressure variation along a compressor flow path for equivalent impeller speeds of 8000 and 10,000 rpm at maximum flow and at peak compressor adiabatic efficiency are shown in figure 12. The static pressures represent an arithmetic average of the inner- and outer-wall measurements along the flow path except for the impeller section, where pressures along only the front cover were measured. The abscissa designates the stations schematically shown in figure 6 and bears no relation to path length or changes in radius. At maximum flow, a large pressure drop occurred near the first static-pressure tap within the vaned-collector passage and indicated that the flow choking point occurred at the inlet to the vaned collector. Performance data showed that this condition was true for all equivalent impeller speeds from 7000 to 10,000 rpm.

Calculated Mach numbers at the point within the vaned-collector passage corresponding to the point of minimum static pressure (station 18 of fig. 12) are presented in figure 13. These Mach numbers were calculated using the form of the Bernoulli equation given in equation (1). Here P is the arithmetic average of the measured total pressure at the inlet to the collector vane as determined by pressure surveys across the flow channel and p is the measured static pressure at station 18 in the vaned-collector passage. For weight flows corresponding to the choking point, Mach numbers of 1.0 were obtained for all equivalent impeller speeds except 5000 rpm, at which a condition of choked flow was never reached. For points along the constant maximum-flow line, Mach numbers greater than 1.0 were obtained. Inasmuch as maximum flow approximately corresponds to a Mach number of 1.0 in the vaned collector, choking near the inlet of the vaned collector was evidently responsible for the flow limitation.

The choking may be attributed to flow separation at the vane inlet, inasmuch as the effective flow area must have been less than the geometric passage area for choking to occur at the maximum observed flow rates. The flow separation may occur either from the outer or inner walls of the channel or from the leading edges of the collector vanes. Figure 14 shows the air-stream Mach number and the angle of attack as determined from surveys across the channel at the inlet to the vane collector. The angle of attack is considered negative when the vector of incoming velocity makes a tangential angle less than the tangential angle of the vane inlet (15° in this case) so that the flow is directed from the high- to the low-pressure sides of the vane, which is opposite to conventional airfoil designation. Curves are presented for surge, peak adiabatic efficiency, and maximum flow at an equivalent impeller speed of 8000 rpm. The curves for the three different flow conditions show that the peak angle of attack and the peak Mach number shift from the inner wall at maximum flow to approximately the center of the passage for peak adiabatic efficiency and surge. The Mach number at the vane inlet for maximum flow is of the order of 0.6, which is relatively low compared with the high Mach-number values at the critical-flow region in the vaned-collector passage and indicates that the air-flow restriction occurred in the short flow-path length between the vane inlet and station 18 (fig. 12). Because a -15° angle of attack represents only rotational flow, figure 14(c) indicates for the choking-flow condition a reversal of the through-flow velocity at the outer passage wall and a piling up of the air on the inner passage wall. This poor mass-flow distribution also results in variations in the angle of attack across the passage, which are apparently too great for a satisfactory inlet air-stream distribution over the vane. The flow separation with the resulting flow restriction in the vaned-collector passage is therefore believed to result from poor distribution of mass flow across the passage at the vane inlet.

Design Changes for Improving Compressor Performance

The design change to increase the flow capacity of the compressor was based on an analysis of the flow at the vaned-collector inlet at maximum weight flow. The exact location of the choking point is a function of the flow conditions and the flow-passage geometry. If it is assumed that the flow from the vaneless diffuser enters the vaned collector tangent to the passage walls and that this flow process takes place isentropically, the flow restriction would occur at the minimum passage area.

If the vaned-collector inlet is assumed to be a nozzle, then by using values of pressure and temperature corresponding to maximum air flow at several impeller speeds it was possible to determine the effective critical throat or nozzle area and to determine whether the geometric throat area could be used as an index of the flow limitations of the compressor. The application of the steady-flow isentropic-energy equation to the data is presented in appendix B.

The calculated effective critical throat areas at maximum weight flow over a range of equivalent impeller speeds from 7000 to 10,000 rpm as shown in figure 15. A constant effective critical throat area of 0.46 square foot was obtained regardless of variations in impeller speed and maximum weight flow. This constant value is 90 percent of the geometric throat area (0.51 sq ft) and indicates that the conception of the vaned-collector inlet as the throat of a nozzle is valid in establishing a useful index of the air-flow capacity of this compressor. The air-flow capacity may then be increased by increasing the geometric flow area at the vaned-collector inlet; the increased air-flow capacity will, however, only be proportionate to the change in passage area when the air density at the passage inlet remains constant. The vaned-collector-inlet area was increased from 0.51 to 0.68 square foot by cutting back the inlet edges of the collector vanes, which resulted in an increased vaneless-diffuser radius. Increasing the air-flow capacity in this manner would also tend to improve the efficiency of the compressor, for such an increase would shift the diffuser performance curve to higher weight flows where the peak efficiency of the impeller occurred.

Revised Compressor

Compressor performance. - The compressor performance characteristics over the range of equivalent impeller speeds from 3600 to 11,500 rpm are shown in figure 16. A maximum adiabatic efficiency of 0.81 was obtained at an equivalent impeller speed of 7000 rpm, a corrected weight flow of 36.5 pounds per second, and a pressure ratio of 1.90. The peak pressure ratio was 3.93 and occurred at an equivalent impeller speed of 11,500 rpm, a corrected weight flow of 65.5 pounds per second, and an adiabatic efficiency of 0.72. The maximum corrected weight flow at 11,500 rpm was 76 pounds per second.

The variations of maximum corrected weight flow in the compressor with equivalent impeller speed for the original and revised compressors are shown in figure 17. Data are not presented for speeds lower than 7000 rpm, inasmuch as choking conditions were never reached in the compressor for these speeds because of capacity limitations of the exhauster system under these operating conditions. The curves of figure 17 show that a considerable increase in maximum corrected weight flow was obtained with the revised compressor over the speed range. The largest increase, 27 percent, occurred at 7000 rpm and the increase at the highest comparative speed, 10,000 rpm, was 12 percent. Extrapolation of the revised compressor-flow curve indicated that at an equivalent impeller speed of 11,500 rpm the design flow of 78 pounds per second would almost be reached. The data point at 11,500 rpm, however, for an inlet-air temperature of -32° F and an inlet-air total pressure of 6 inches of mercury absolute was approximately 2.5 percent lower than the extrapolated value for this speed.

In order to determine some of the effects of inlet conditions on compressor performance, an investigation was made at an equivalent impeller speed of 8000 rpm for different inlet-air temperatures and pressures. Figure 18 shows the variation of compressor adiabiatic efficiency and total-pressure ratio with weight flow for three different inlet conditions. No appreciable change in total-pressure ratio was noted with change in inlet conditions, but a definite drop in efficiency was observed at an inlet-air temperature of -32° F. This reduction in efficiency has been noted by other investigators (reference 5) and is generally attributed to the effect of increased heat transfer. Decreasing the inlet-air pressure from 14 to 8 inches of mercury absolute at constant temperature had a negligible effect on compressor efficiency. The maximum weight flow was decreased approximately 3 percent when both the inlet-air pressure and temperature were reduced and approximately 2 percent when the inlet-air pressure alone was reduced. These values are of about the same magnitude as suggested by the extrapolation of the weight-flow curve of figure 17. In general, a change in inlet-air pressure had more effect on maximum weight flow than a change in inlet-air temperature and a reduction in either resulted in slightly lower values of the air flow.

Compressor-component performance. - The performance of the compressor, the impeller, and the diffuser is shown in figure 19. For equivalent impeller speeds from 3600 to 8000 rpm, the impeller efficiencies were high and had a comparatively constant value over the flow range with a maximum value of 0.95 being reached at 3600 rpm. At speeds from 8000 to 11,500 rpm, the impeller performance curves considerably decreased with increased weight flow; an efficiency of 0.62 was obtained at maximum flow at the design speed of 11,500 rpm. The rapid decrease in impeller efficiency at high-flow, high-speed conditions indicated that pressure losses preliminary to choking in the impeller were being encountered.

In general, the peak diffuser efficiency occurred at approximately the center of the flow range at each speed. Peak diffuser efficiencies varied somewhat over the speed range; a maximum value of 0.78 occurred at an equivalent speed of 11,500 rpm. At similar values of air flow, the revised compressor generally had higher efficiencies than the original compressor. The useful range of operation of the revised compressor was shifted to higher values of air flow than with the original compressor, thus showing that altering the vaned collector resulted in improved matching of the impeller and diffuser components.

Flow capacity and limitations. - The static-pressure variation through the revised compressor is shown in figure 20 for peak efficiency and maximum weight flow at equivalent impeller speeds of 8000, 10,000, and 11,500 rpm. For peak efficiency, a steady pressure rise in general occurred through the impeller, vaneless diffuser, and vaned collector.

The curves show that for maximum flow a pressure loss occurred near the impeller inlet and in the vaned collector. The largest pressure drop occurred in the vaned collector and, as in the original compressor, was a result of choking in this component. The minimum pressure in the vaned collector was reached approximately one-third the distance of the flow path through the vaned collector. In general, about 50 to 65 percent of this static-pressure drop in the vaned collector was recovered by the time the air had reached the burner annulus.

A study of the maximum-flow curves in figure 20 shows that with an increase in speed the pressure drop near the impeller inlet became larger. At an equivalent impeller speed of 11,500 rpm, compression in the impeller started with a static pressure approximately 40 percent below the static pressure at the impeller inlet,

Considering the concept of the vaned-collector inlet as the throat of a nozzle, the effective critical throat areas were calculated over an equivalent impeller speed range from 7000 to 11,500 rpm according to the method presented in appendix B. The calculated effective critical throat areas for both the original and revised compressors are shown in figure 21. The revised compressor had an approximately constant effective critical throat area of 0.64 square foot (94 percent of the geometric throat area). The ratio of the maximum corrected weight flows of the revised compressor to the maximum corrected weight flows of the original compressor is shown in figure 22 over a range of equivalent impeller speeds from 7000 to 10,000 rpm. The ratio of effective critical throat areas of the two compressors is also given in figure 22. The weight-flow-ratio curve is considerably lower than the area-ratio curve at 7000 rpm and the difference between the two curves rapidly increases as the speed is increased. This fact together with a study of equation (4) (appendix B) suggests that either the total-pressure or the total-temperature at the throat of the revised vaned collector had been adversely affected at some point in the compressor system prior to the throat section.

The impeller-outlet total-pressure ratios and total-temperature ratios for both compressors over a range of speeds at maximum flow are shown in figure 23. The curves show slightly lower impeller-outlet temperature ratios for the revised compressor than for the original compressor, but these lower temperature ratios are accompanied by large reductions in impeller-outlet total-pressure ratios. At an equivalent impeller speed of 10,000 rpm, the impeller-outlet total-pressure ratio for the revised compressor was 78 percent of that obtained for the original compressor. The reductions in total pressure were due to pressure losses in the impeller near the impeller inlet at high flows and explain why the increase in weight flow with the revised compressor was disproportionate to the increased effective critical flow area. In reference 6, impeller-inlet pressure losses were shown to be critically affected by both blade angle of attack and blade Mach number. This impeller has relatively high blade-inlet Mach numbers with resulting limitations on the blade-inlet angle design. The undesirable pressure losses could possibly be reduced by altering the inlet edge of the impeller blades to give an impeller of increased design air-flow capacity.

The maximum corrected weight flow obtained over a range of equivalent impeller speeds for the original compressor, the revised compressor, and a theoretical compressor consisting of the revised vaned collector and vaneless diffuser with a hypothetical impeller is shown in figure 24. This impeller component was assumed to have, at maximum flow, the peak impeller pressure ratio and peak impeller efficiency experimentally obtained on the revised compressor. From equation (4) (appendix B), the pressures and temperatures corresponding to peak impeller efficiency and pressure ratio, and the effective critical throat area of 0.64 square foot, the maximum corrected weight flows were obtained for the theoretical compressor. At a speed of 11,500 rpm with the theoretical compressor, the weight-flow capacity could be increased from 76 pounds per second with the revised compressor to 112 pounds per second, a 47-percent increase. This optimum value of 112 pounds per second would require that the impeller have the high specific flow capacity of 12,300 cubic feet per minute per square foot. In any attempt to increase the pressure ratio and maximum weight flow of the compressor, the impeller component must be modified to eliminate the pressure losses therein.

SUMMARY OF RESULTS

In the investigation of the component and over-all performance of a large centrifugal compressor and a revised compressor, the following results were obtained:

1. The flow capacity of the original compressor up to an equivalent speed of 10,000 rpm (speed limited by mechanical failure) was limited by choking in the vaned collector. The maximum flow values indicated that the compressor design flow at rated equivalent speed of 11,500 rpm would not be attained.

2. Revision of the vaned collector resulted in an increased air-flow capacity over the speed range. The design air flow of 78 pounds per second was very nearly reached for the revised compressor at rated engine speed of 11,500 rpm.

3. At similar values of air flow, the revised compressor generally had higher efficiencies than the original compressor and the useful range of operation of the revised compressor was shifted to higher values of air flow, which showed that altering the vaned collector resulted in improved matching of the impeller and diffuser components.

4. For the revised compressor, a maximum adiabatic efficiency of 0.81 was obtained at an equivalent impeller speed of 7000 rpm, a corrected weight flow of 36.5 pounds per second, and a pressure ratio of 1.90. The peak pressure ratio was 3.93 and occurred at an equivalent impeller speed of 11,500 rpm and a corrected weight flow of 65.5 pounds per second.

5. Decreasing the compressor-inlet-air temperature decreased the compressor efficiency and the maximum corrected weight flow. Decreasing the compressor-inlet-air pressure had no appreciable effect on the compressor efficiency or pressure ratio but did decrease the maximum weight flow.

6. At maximum flow, the original compressor utilized approximately 90 percent of the available geometric passage throat area and the revised compressor utilized approximately 94 percent, regardless of impeller speed.

7. The ratio of the maximum weight flows of the revised and original compressors was less than the ratio of the effective critical throat areas of the two compressors because of large pressure losses in the impeller near the impeller inlet and the difference increased with an increase in impeller speed. In any attempt to increase further the pressure ratio and maximum weight flow of the compressor, the impeller must be modified to eliminate these pressure losses.

8. A theoretical compressor consisting of the revised vaned collector and vaneless diffuser with an impeller advantageously combining peak impeller pressure ratio and peak impeller efficiency at maximum flow would be capable of producing a maximum corrected air flow of 112 pounds per second at an equivalent impeller speed of 11,500 rpm.

Lewis Flight Propulsion Laboratory,
National Advisory Committee for Aeronautics,
Cleveland, Ohio.

APPENDIX A

SYMBOLS

The following symbols are used in this report:

A	nozzle area, sq ft
M	Mach number
N	actual impeller speed, rpm
P	stagnation or total pressure, in. Hg absolute
p	static pressure, in. Hg absolute
Q	$\frac{\text{static pressure in simulated burner annulus}}{\text{static pressure at impeller outlet}}$
T	total temperature, °R
W	air weight flow at inlet conditions, lb/sec
γ	ratio of specific heats
δ	ratio of actual inlet stagnation pressure to standard sea-level pressure
η_{ad}	adiabatic efficiency
θ	ratio of actual inlet stagnation absolute temperature to standard sea-level absolute temperature

Subscripts:

0	compressor inlet
1	impeller outlet
2	vaneless-diffuser outlet
3	nozzle throat
4	simulated-burner annulus
max	maximum

APPENDIX B

DETERMINATION OF EFFECTIVE CRITICAL THROAT AREA AT VANED-COLLECTOR INLET

The steady-flow isentropic energy equation for a nozzle can be expressed as

$$W = 145.8 \frac{A_3 P_2}{\sqrt{T_2}} \sqrt{\left(\frac{p_3}{P_2}\right)^{\frac{2}{\gamma}} - \left(\frac{p_3}{P_2}\right)^{\frac{\gamma+1}{\gamma}}} \tag{2}$$

The maximum weight flow through the nozzle will be reached when the critical pressure occurs in the throat section and equation (2) reduces to

$$W_{max} = 37.6 \frac{A_3 P_2}{\sqrt{T_2}} \tag{3}$$

Because the air-flow data are presented corrected to standard sea-level pressure and temperature at the compressor inlet, the same procedure will be followed here. Equation (3) is then expressed

$$A_3 = \frac{\left(\frac{W_{max}\sqrt{\theta}}{\delta}\right)\sqrt{T_2/T_0}}{49.5\left(\frac{P_2}{P_0}\right)} \tag{4}$$

In applying equation (4) to the data, T_2 is assumed equal to the total temperature measured in the simulated burner annulus T_4 and P_2 is assumed equal to the total pressure at the impeller tip P_1 calculated according to the method previously described. The results of several check runs at maximum-flow conditions with a total-pressure probe in the vaneless diffuser near the vaned-collector inlet of both the original and the revised compressors showed that a negligible difference existed between the calculated impeller-outlet pressures and the pressure-probe readings.

REFERENCES

1. Ellerbrock, Herman H., Jr., and Goldstein, Arthur W.: Principles and Methods of Rating and Testing Centrifugal Superchargers. NACA ARR, Feb. 1942.

2. NACA Subcommittee on Supercharger Compressors: Standard Procedures for Rating and Testing Centrifugal Compressors. NACA ARR No. E5F13, 1945.

3. Fechheimer, Carl J.: Measurement of Static Pressure. Mech. Eng., vol. 49, no. 8, Aug. 1927, pp. 871-873; discussion, pp. 873-874.

4. NACA Subcommittee on Compressors: Standard Procedures for Rating and Testing Multistage Axial-Flow Compressors. NACA TN No. 1138, 1946.

5. Anderson, Robert J., Ritter, William K., and Parsons, Shirley R.: Apparent Effect of Inlet Temperature on Adiabatic Efficiency of Centrifugal Compressors. NACA TN No. 1537, 1948.

6. Ginsburg, Ambrose, Ritter, William K., and Palasics, John: Effects on Performance of Changing the Division of Work between Increase of Angular Velocity and Increase of Radius of Rotation in an Impeller. NACA TN No. 1216, 1947.

TABLE I. - STATIC-PRESSURE MEASUREMENT STATIONS ON ORIGINAL AND REVISED COMPRESSORS

Location	Direction and distribution		Reference figure	Station		Original compressor		Revised compressor	
				Original compressor	Revised compressor	Number of stations on outer wall	Number of stations on inner wall	Number of stations on outer wall	Number of stations on inner wall
Along compressor front cover	Equally spaced along profile in axial plane		5(a) and 6	1-12	1-12	12	0	12	0
At impeller inlet on front cover	At same radial distance and 90° on each side of station 12		5(a) ------	12(a) 12(b)	None	2	0	0	0
On vaneless-diffuser section	Along radial lines 180° apart	Right side	5(a) and 6	13-17	None	5	5	0	0
		Left side	5(a) and 6	13-17	13-17	5	5	5	5
Along passage walls of vaned collector	Following mean flow path along increasing and decreasing radius of vaned collector		5(a), 5(b), and 6	18-27	18-26	10	10	9	9
Around periphery at vaned-collector inlet	120° apart and about in center of a passage inlet		5(a) 5(a) ------	17(a) 17(b) 17(c)	None	3	3	0	0
Around periphery at vaned-collector outlet	30° apart and about in center of each passage outlet		5(b)	A-L	A	12	12	1	1
Burner annulus	Equally spaced around periphey of inner wall; single tap on outer wall		6	28	28	1	4	1	4

946

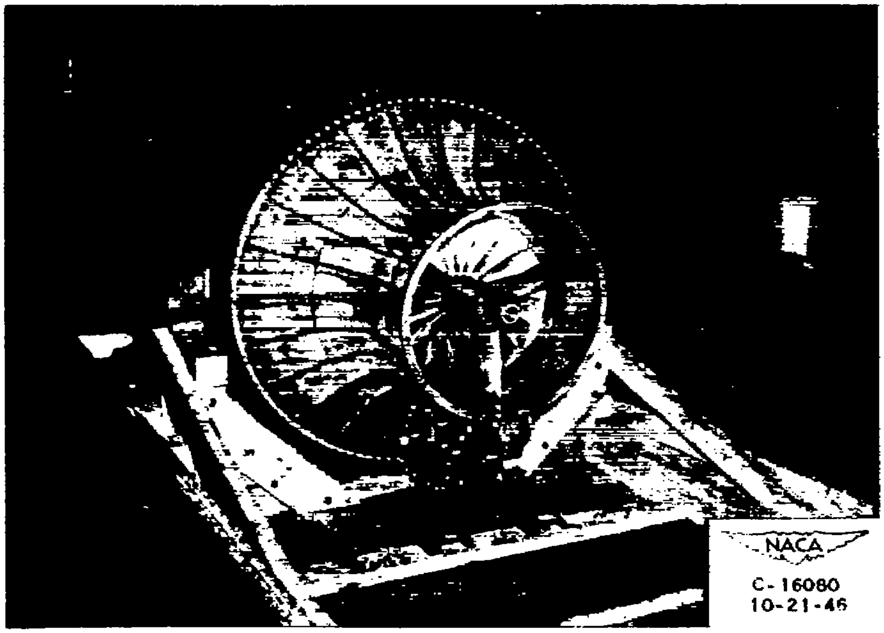
NACA
C-16080
10-21-46

(a) Front view.

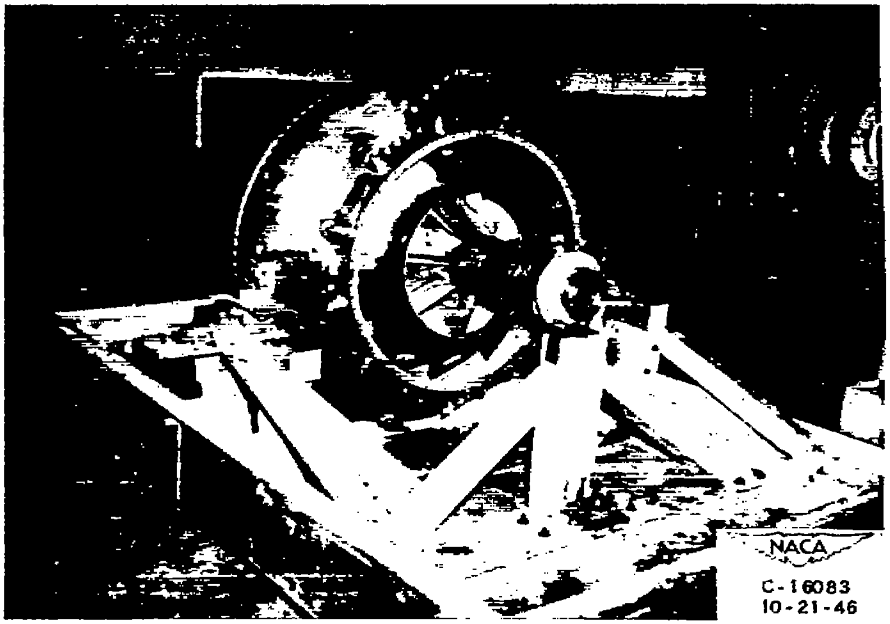
NACA
C-16083
10-21-46

(b) Rear view.

Figure 1. - Original compressor.

966

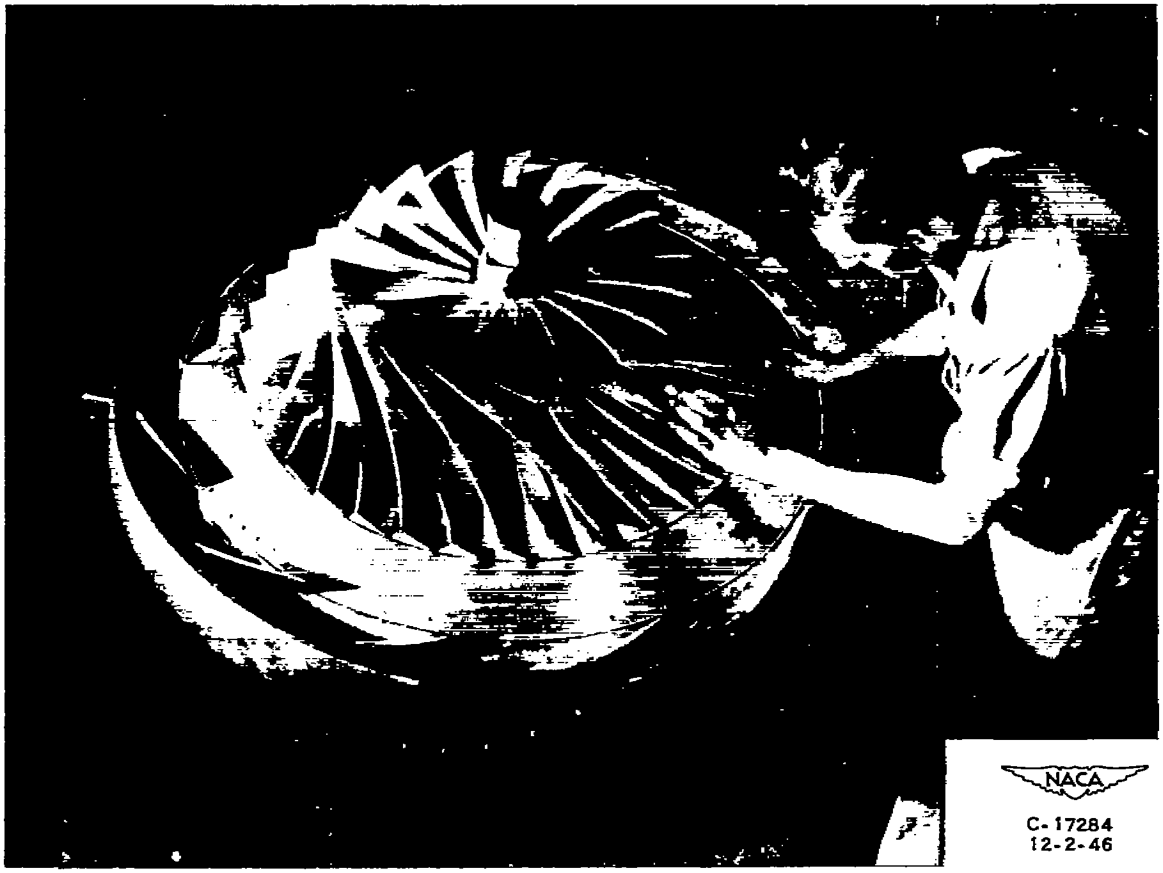

NACA
C-17284
12-2-46

Figure 2. - Impeller and vaned-collector inlet of original compressor.

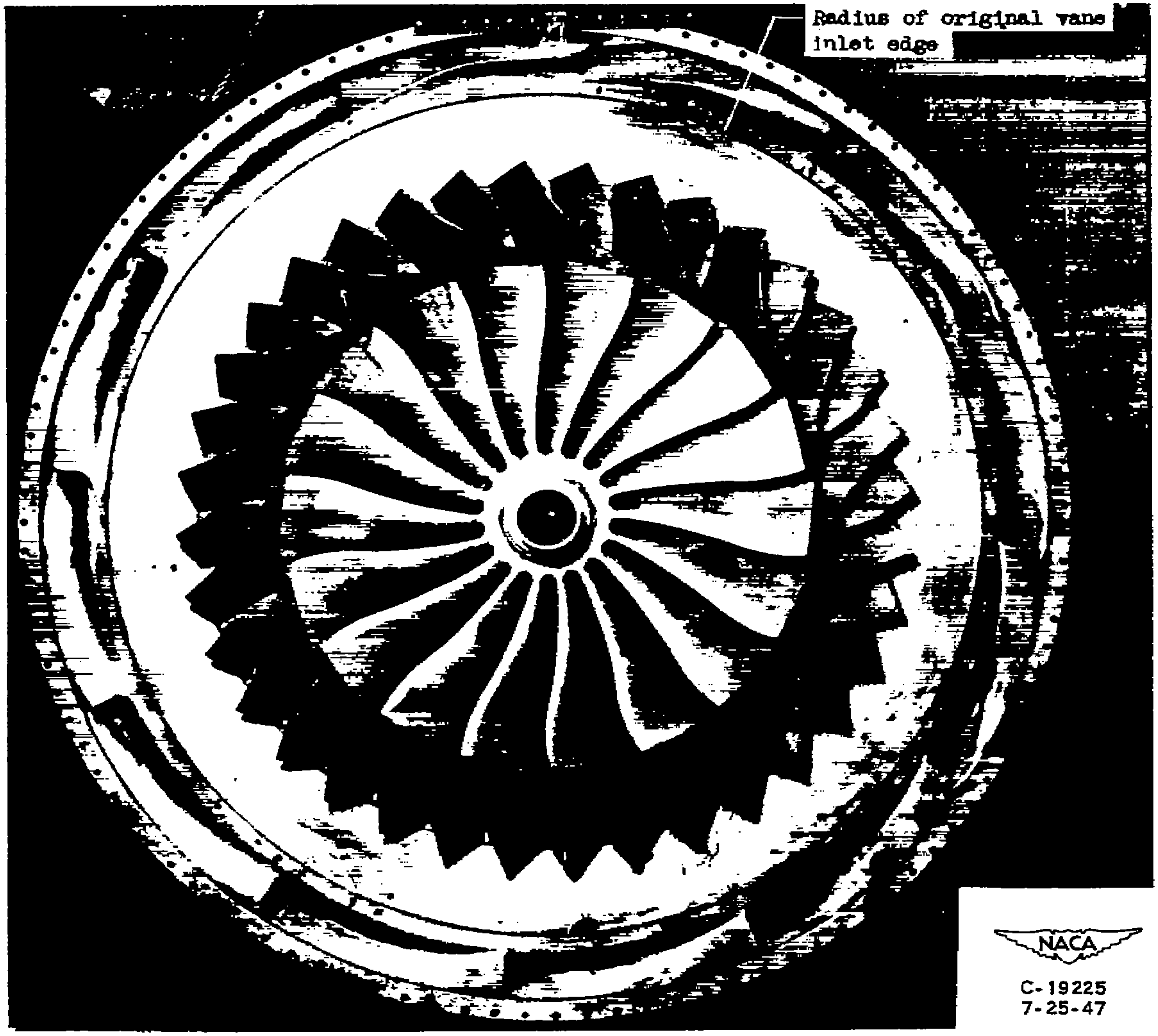
Radius of original vane inlet edge
NACA
C-19225
7-25-47

Figure 3. - Impeller and vaned-collector inlet of revised compressor.

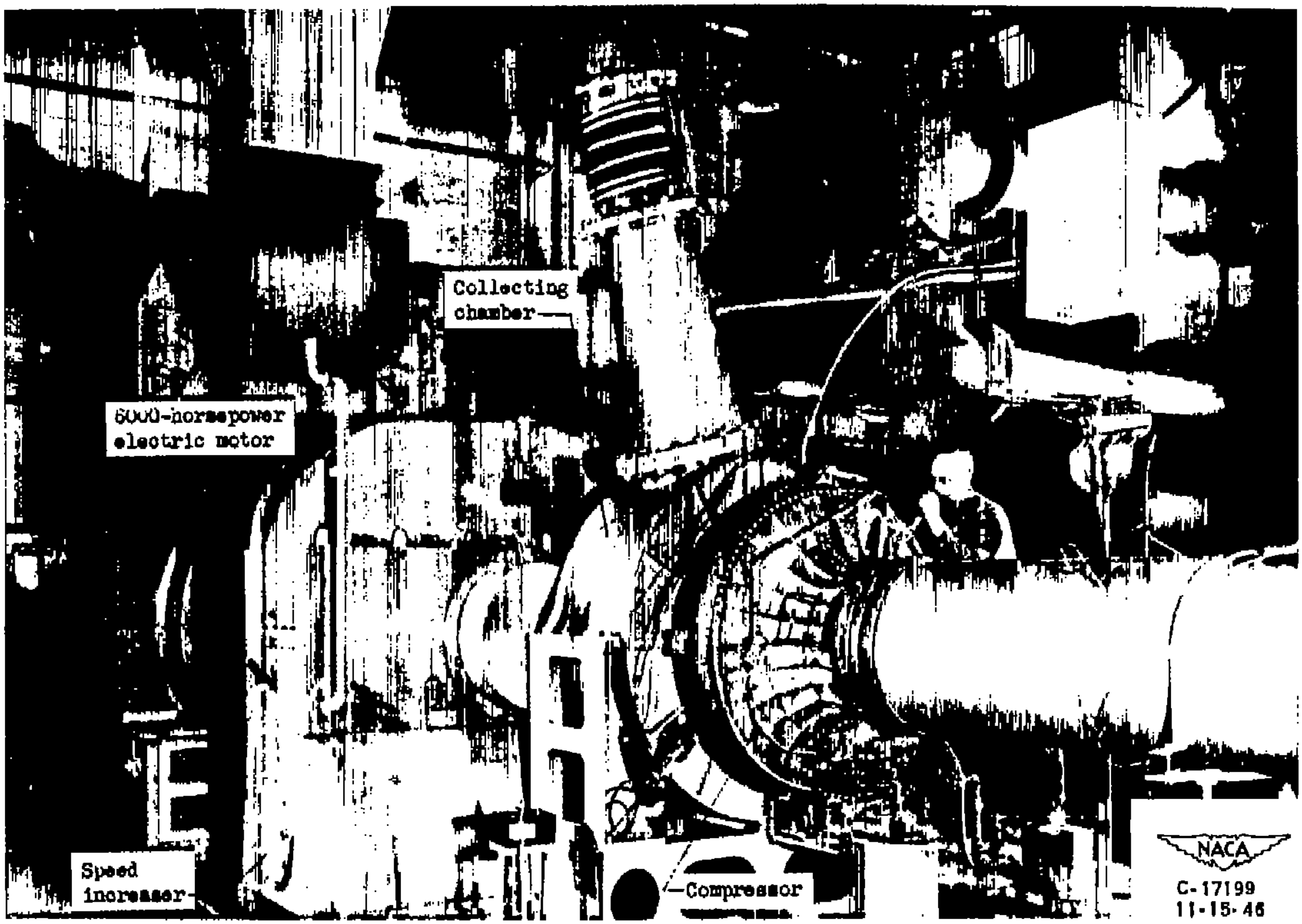
Collecting chamber
6000-horsepower electric motor
Speed increaser
Compressor
NACA
C-17199
11-15-46

Figure 4. - Installation for performance investigation of turbojet-engine compressor.

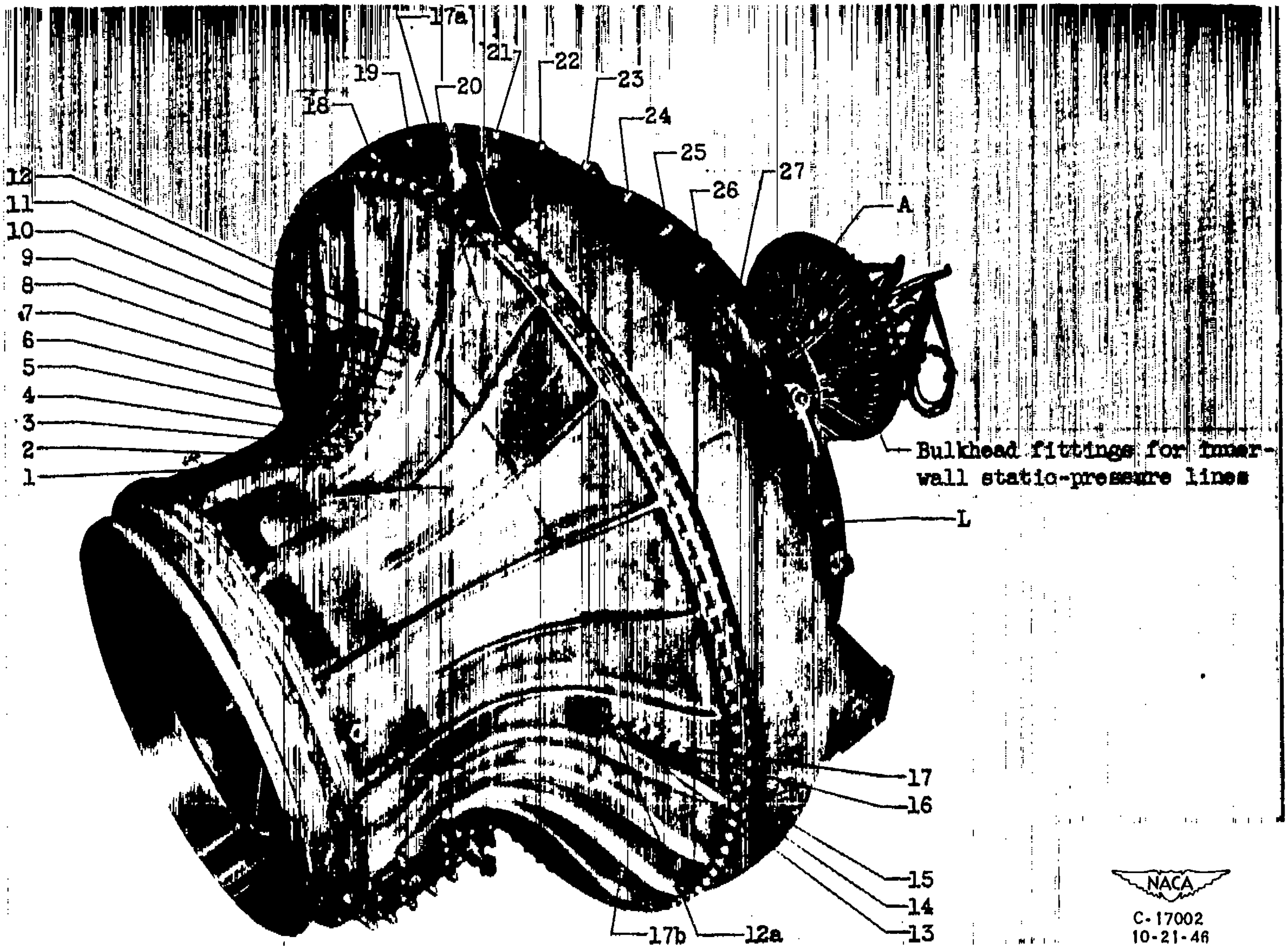
17a
21
19
20
22
23
18
24
25
12
26
27
11
A
10
9
8
7
6
5
4
3
2
1
Bulkhead fittings for inner-wall static-pressure lines
L
17
16
15
14
17b
12a
13
NACA
C-17002
10-21-46

(a) Front view.

Figure 5. - Original compressor showing location of static-pressure stations.

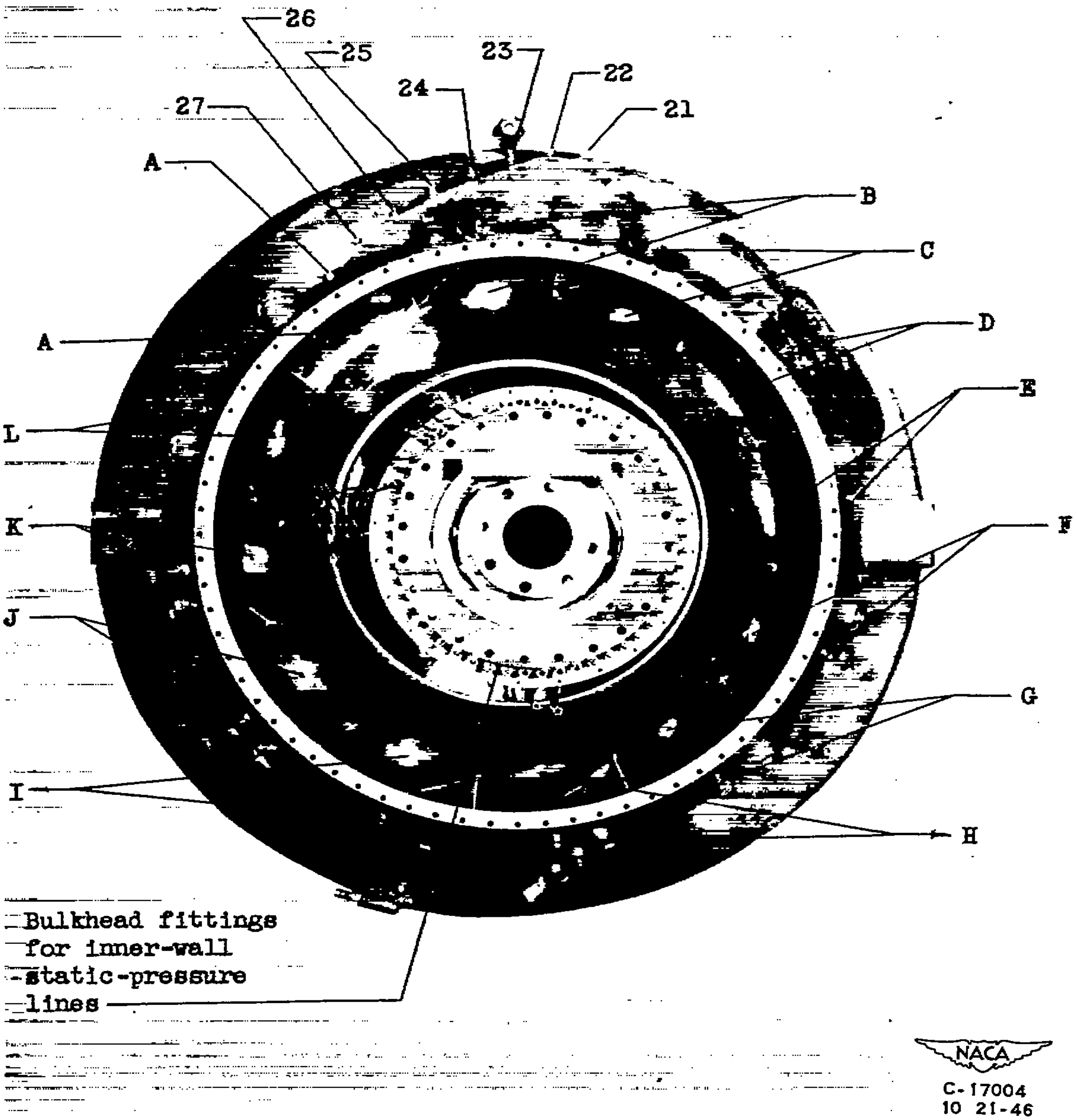

26
25
23
22
24
21
27
A
B
C
A
D
E
L
K
F
J
G
I
H
Bulkhead fittings for inner-wall static-pressure lines
NACA
C-17004
10 21-46

(b) Rear view.

Figure 5. - Concluded. Original compressor showing location of static-pressure stations.

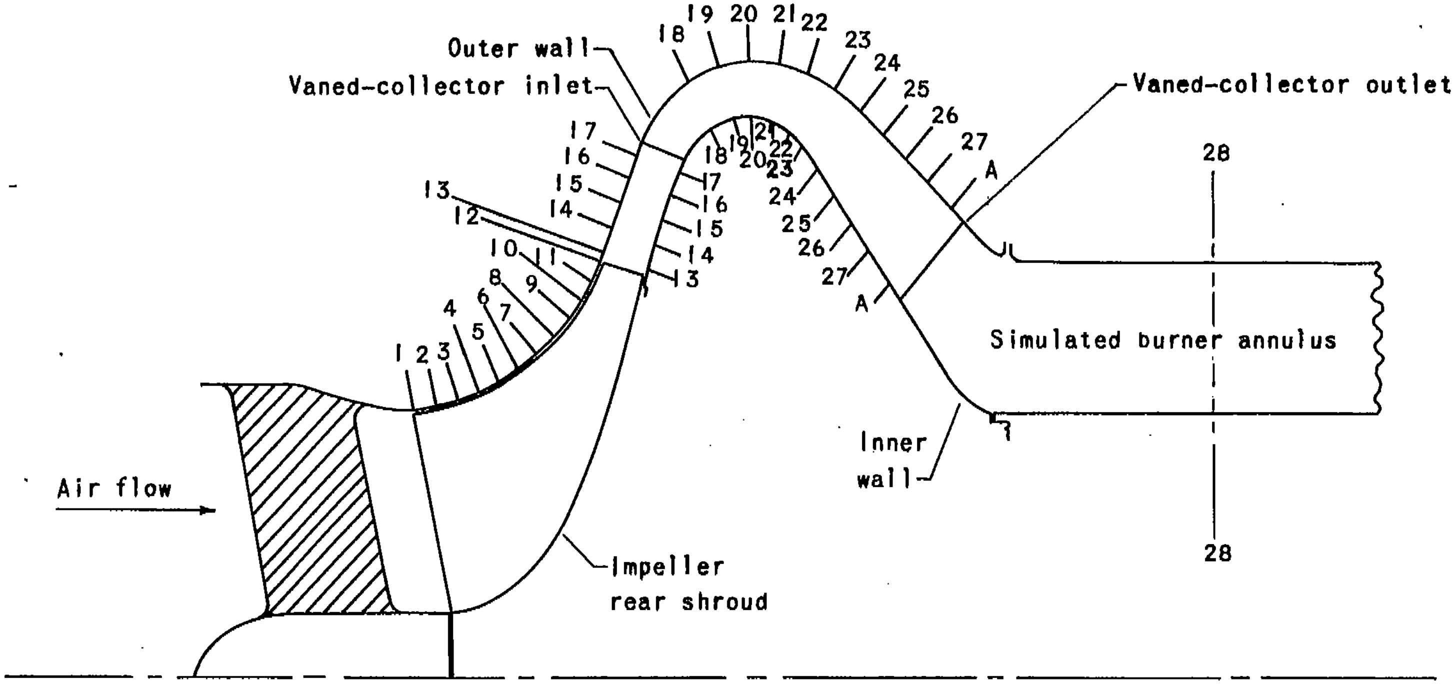
Outer wall
Vaned-collector inlet
Vaned-collector outlet
1
2
3
4
5
6
7
8
9
10
11
12
13
14
15
16
17
18
19
20
21
22
23
24
25
26
27
A
28
Simulated burner annulus
Inner wall
Impeller rear shroud
Air flow

Figure 6. - Schematic diagram of location of static-pressure stations along a flow path in original compressor.

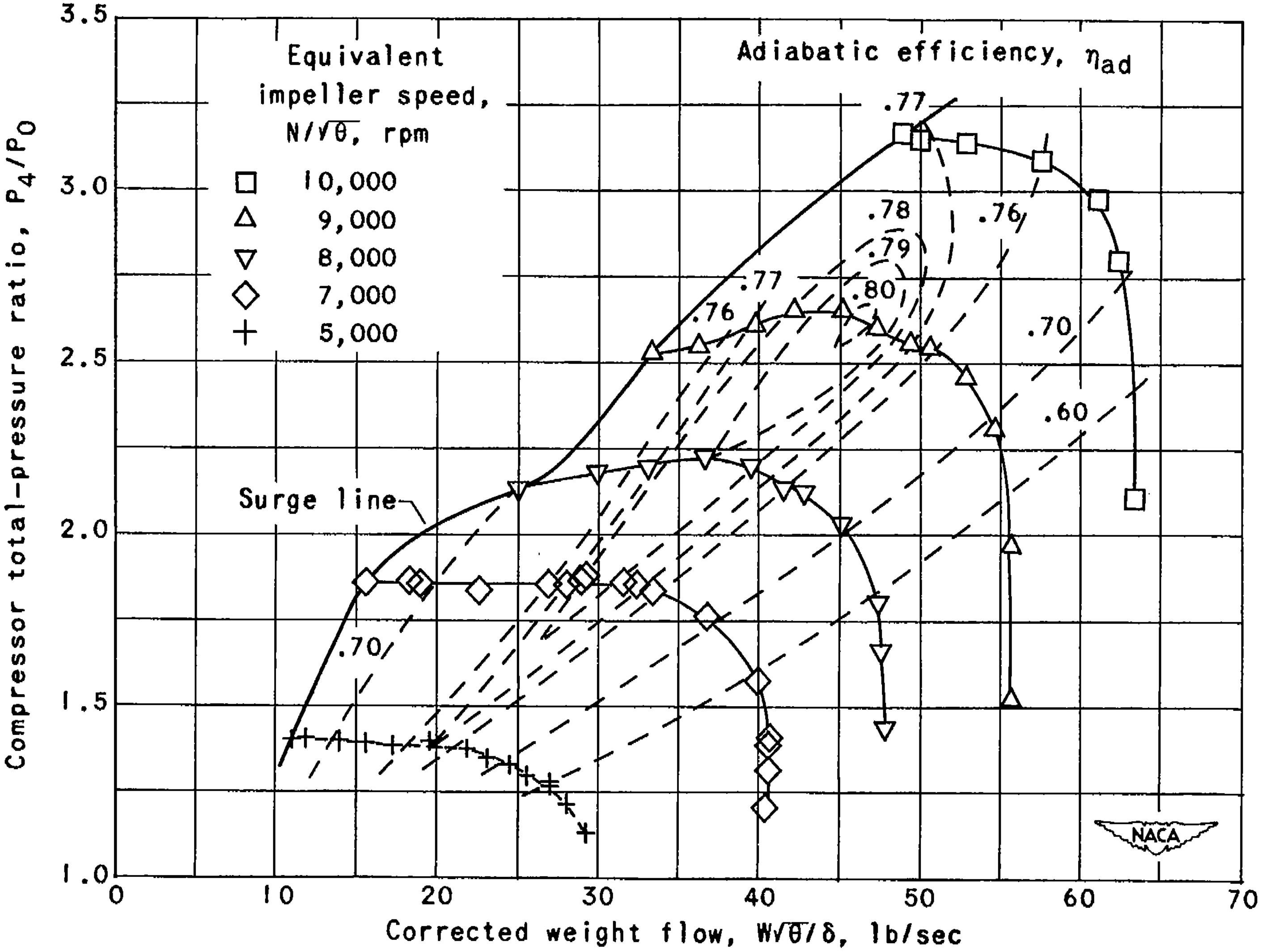

Figure 7. - Performance of original compressor.

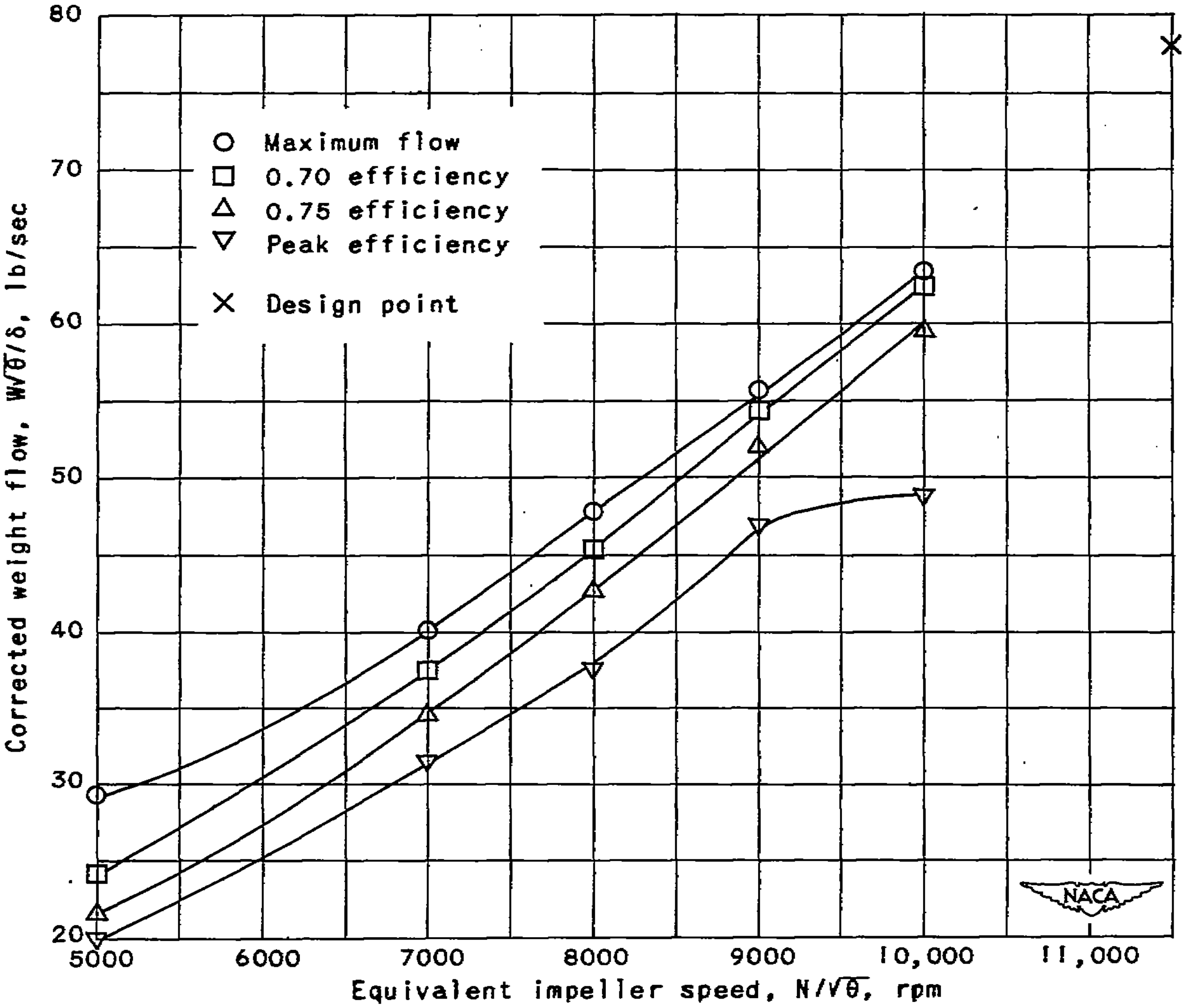

Figure 8. - Variation of weight flow with equivalent impeller speed for several compressor operating conditions. Original compressor.

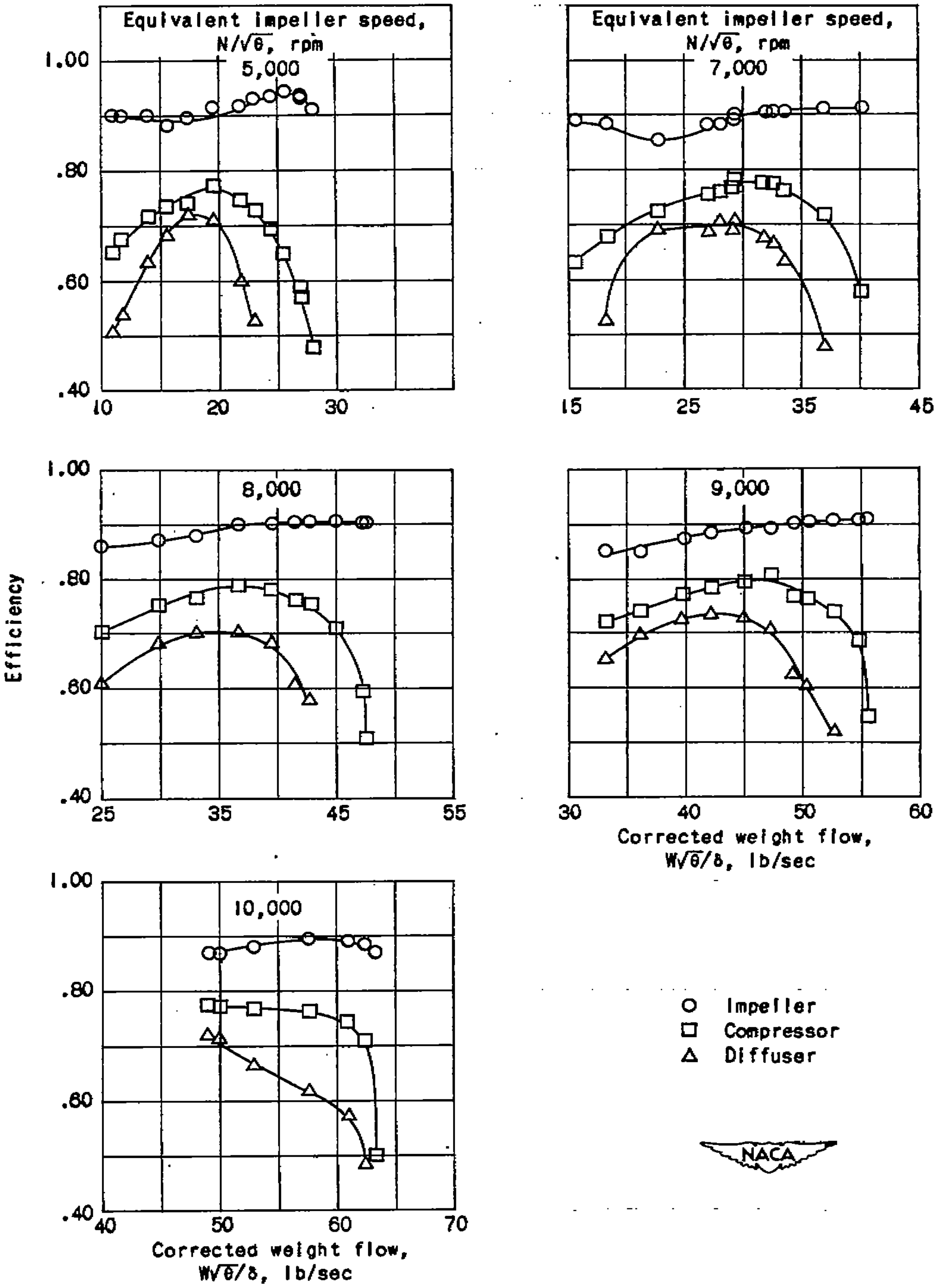

Figure 9. - Performance comparison of compressor, impeller, and diffuser for several impeller speeds. Original compressor.

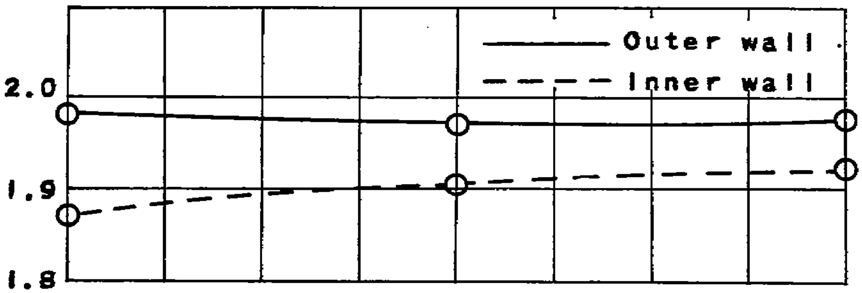

(a) Maximum flow.

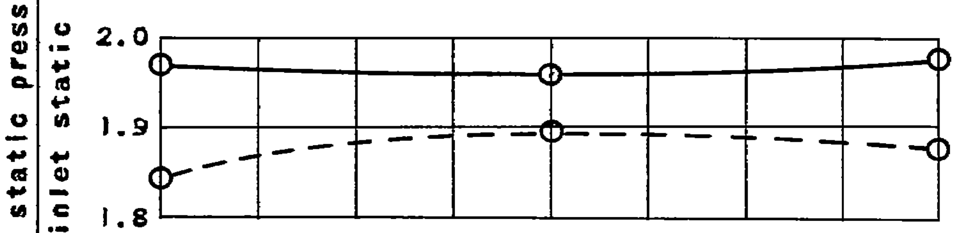

(b) Peak adiabatic efficiency.

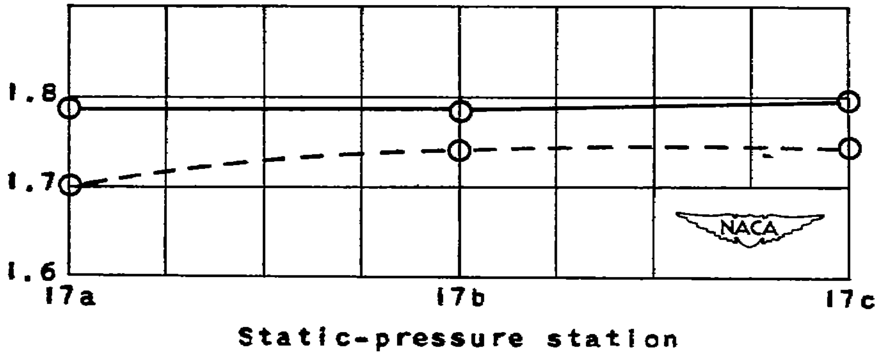

(c) Flow near surge.

Figure 10. - Static-pressure-ratio variation around periphery at vaned-collector inlet. Original compressor; equivalent impeller speed $N/\sqrt{\theta}$, 8000 rpm.

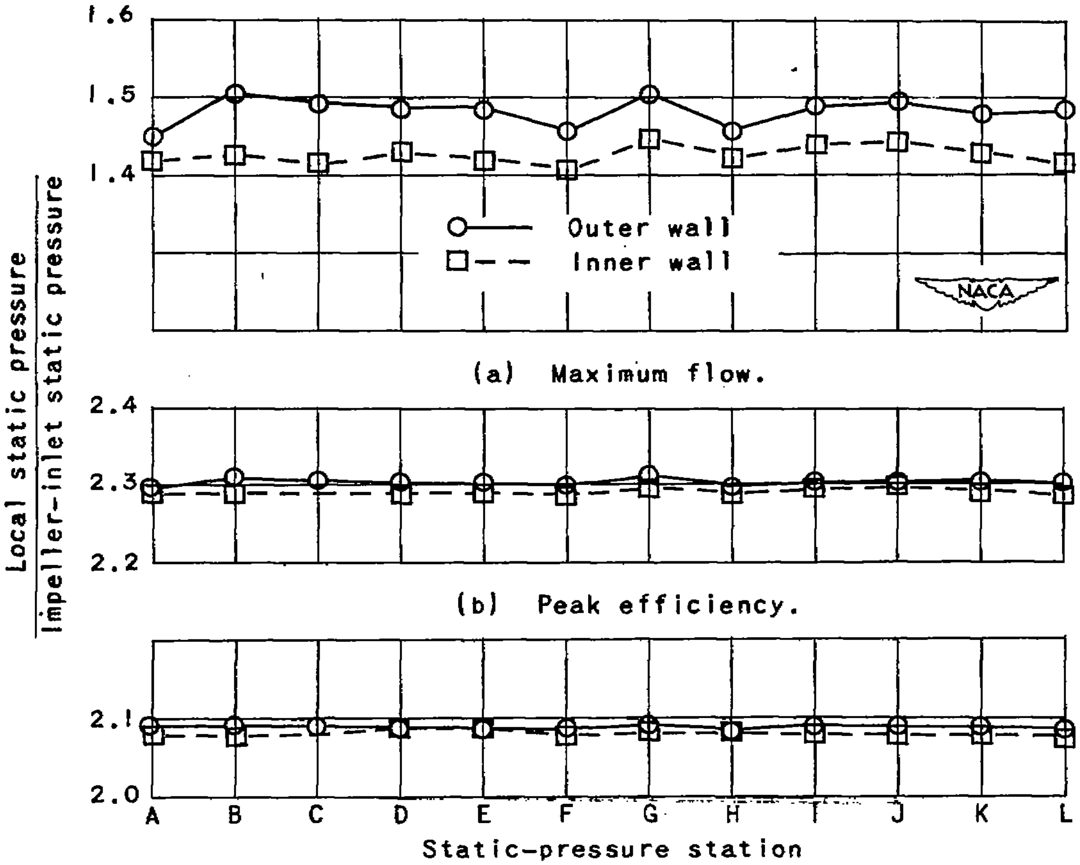

(a) Maximum flow.

(b) Peak efficiency.

(c) Flow near surge.

Figure 11. - Static-pressure-ratio variation around periphery at vaned-collector outlet. Original compressor; equivalent impeller speed $N/\sqrt{\theta}$, 8000 rpm.

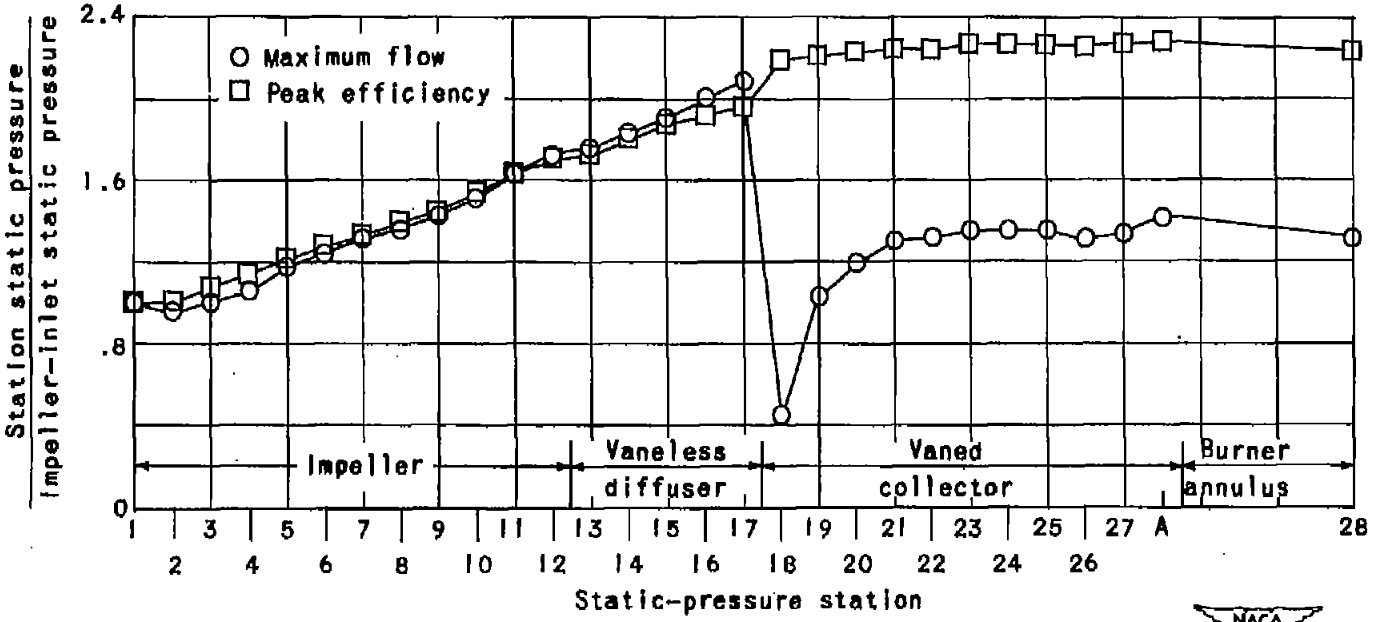

(a) Equivalent impeller speed $N/\sqrt{\theta}$, 8000 rpm.

Figure 12. - Static-pressure variation along compressor flow path. Original compressor.

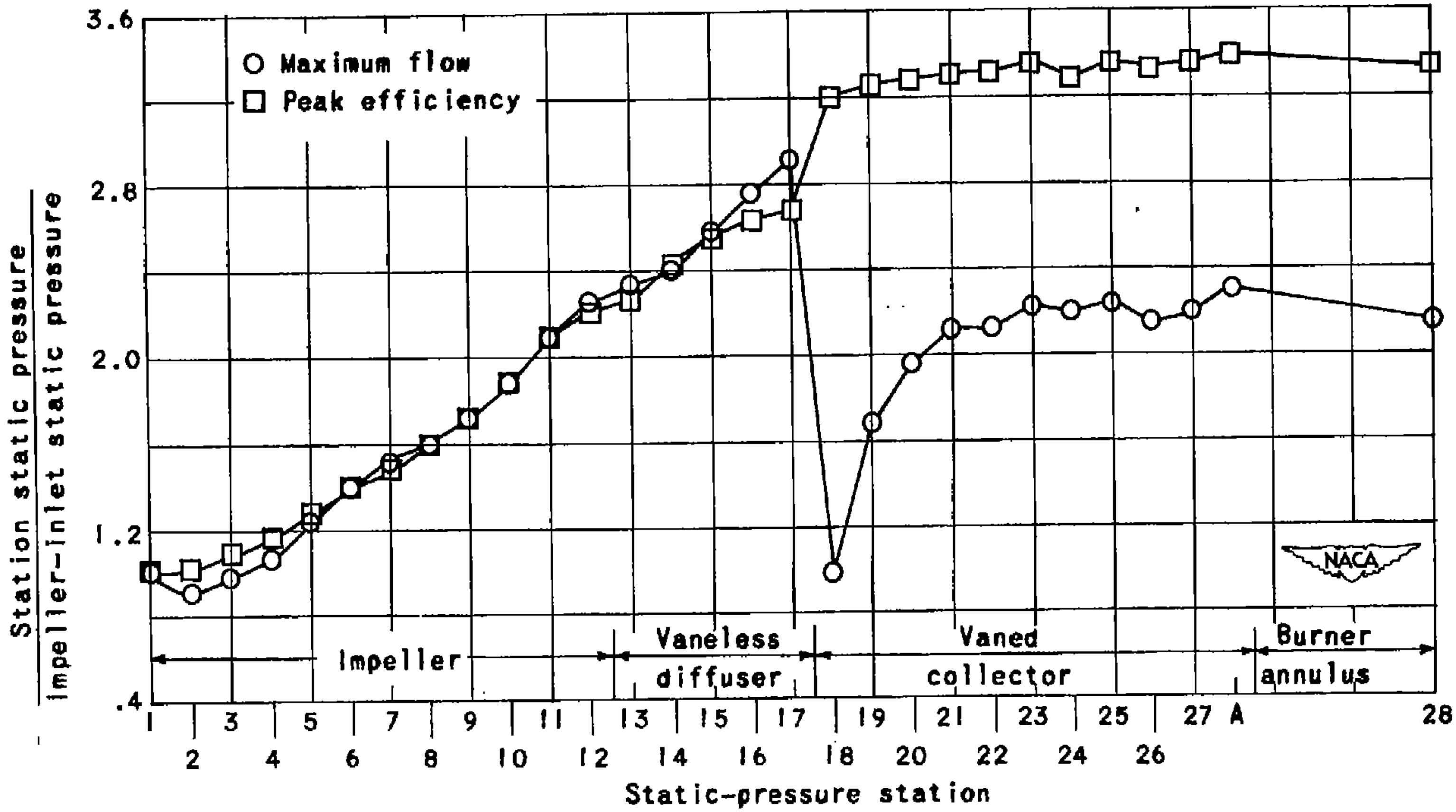

(b) Equivalent impeller speed $N/\sqrt{\theta}$, 10,000 rpm.

Figure 12. - Concluded. Static-pressure variation along compressor flow path. Original compressor.

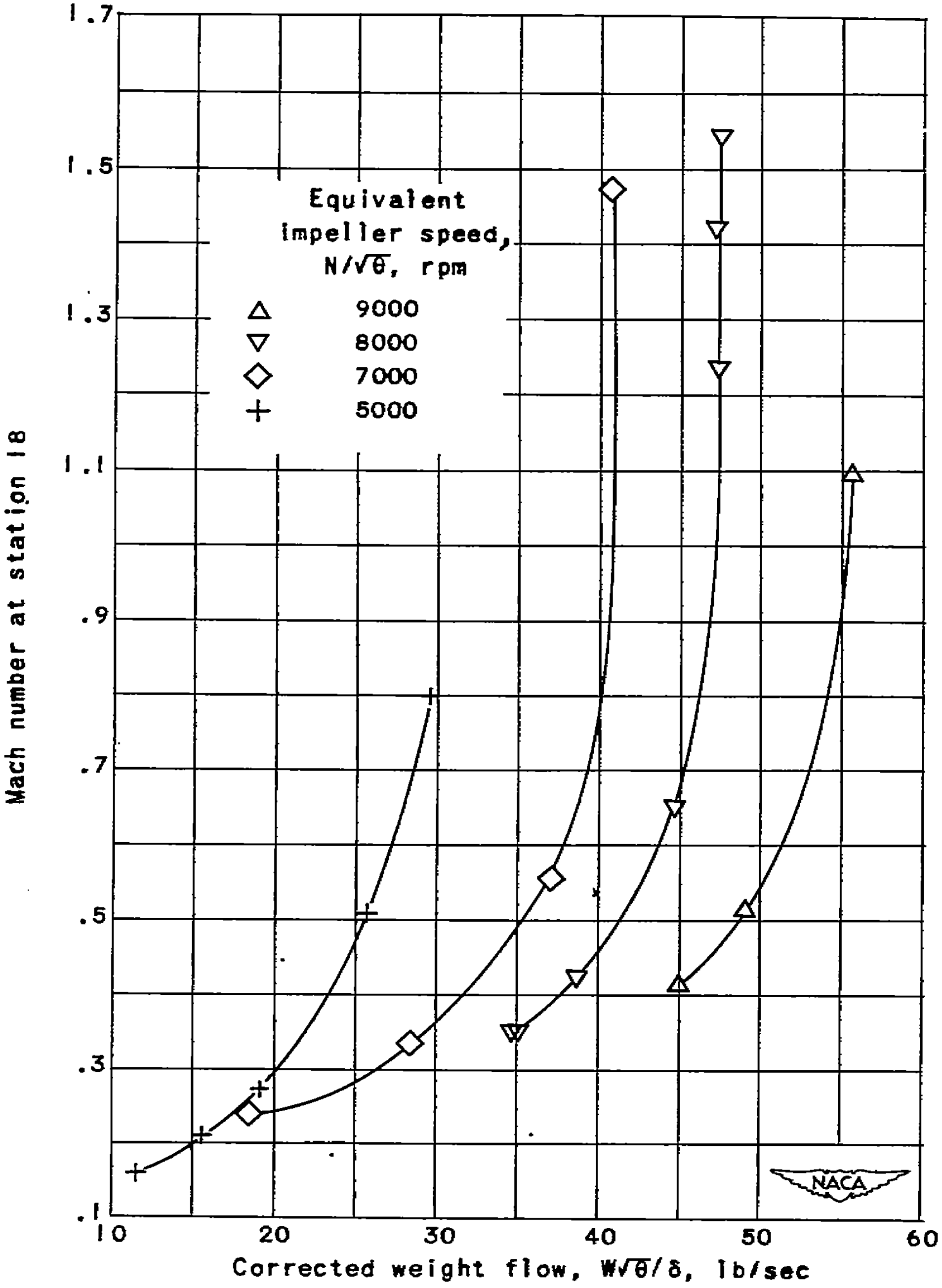

Figure 13. – Relation between Mach number near vaned-collector inlet and compressor weight flow. Original compressor.

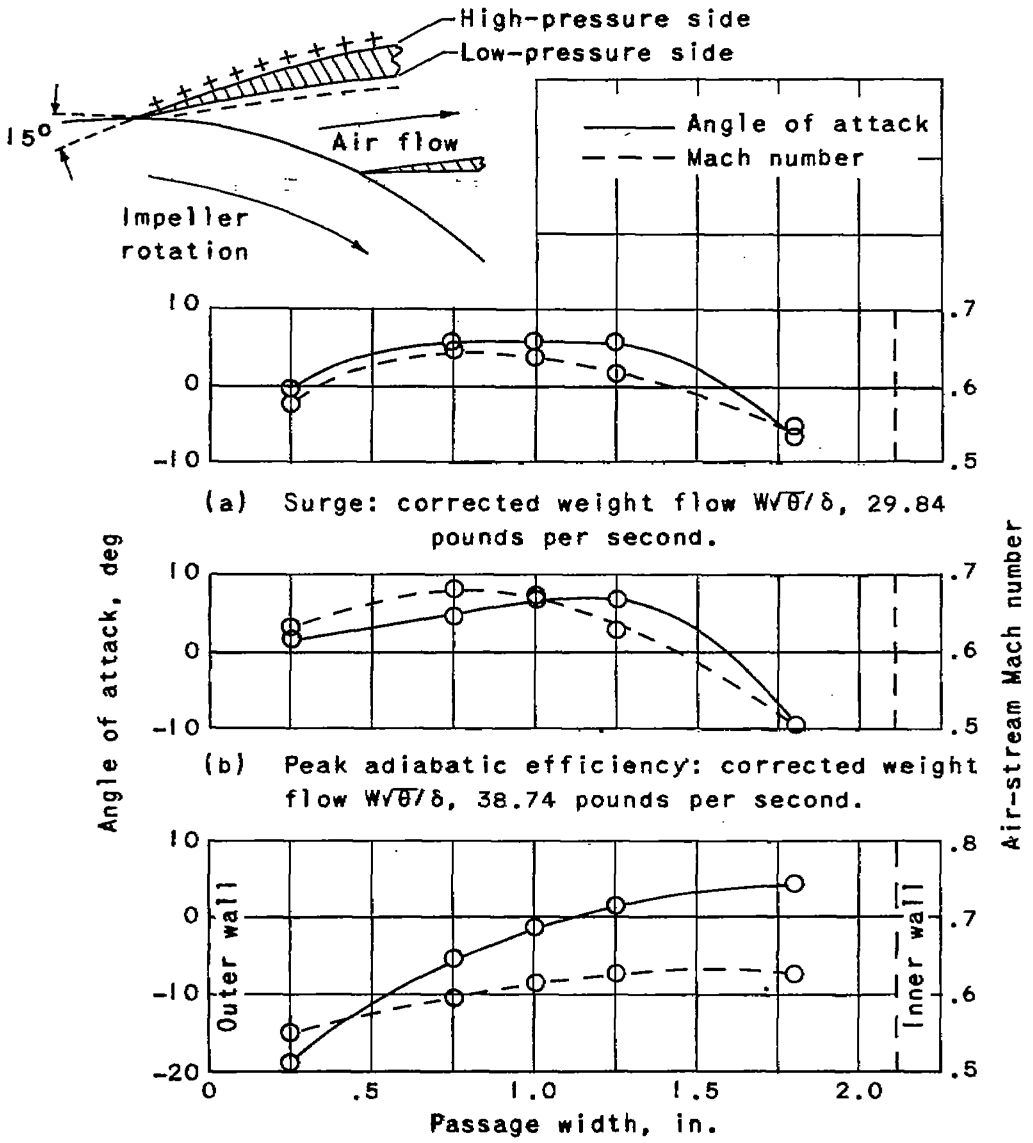

(a) Surge: corrected weight flow $W\sqrt{\theta}/\delta$, 29.84 pounds per second.

(b) Peak adiabatic efficiency: corrected weight flow $W\sqrt{\theta}/\delta$, 38.74 pounds per second.

(c) Maximum flow: corrected weight flow $W_c\sqrt{\theta}/\delta$, 47.29 pounds per second.

Figure 14. - Air-stream surveys at inlet to vaned collector at equivalent impeller speed of 8000 rpm for various flow conditions. Original compressor.

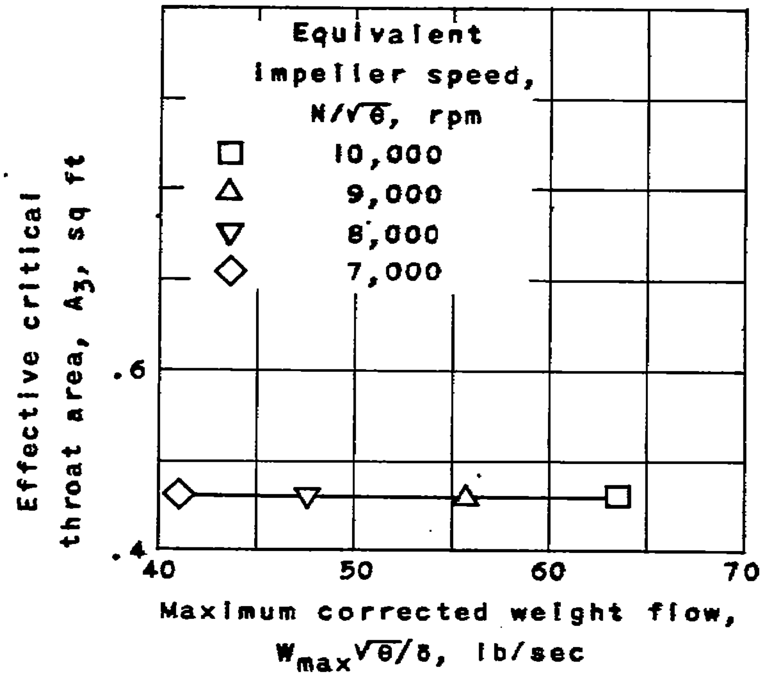

Figure 15. - Variation of effective critical throat area with maximum corrected weight flow. Original compressor.

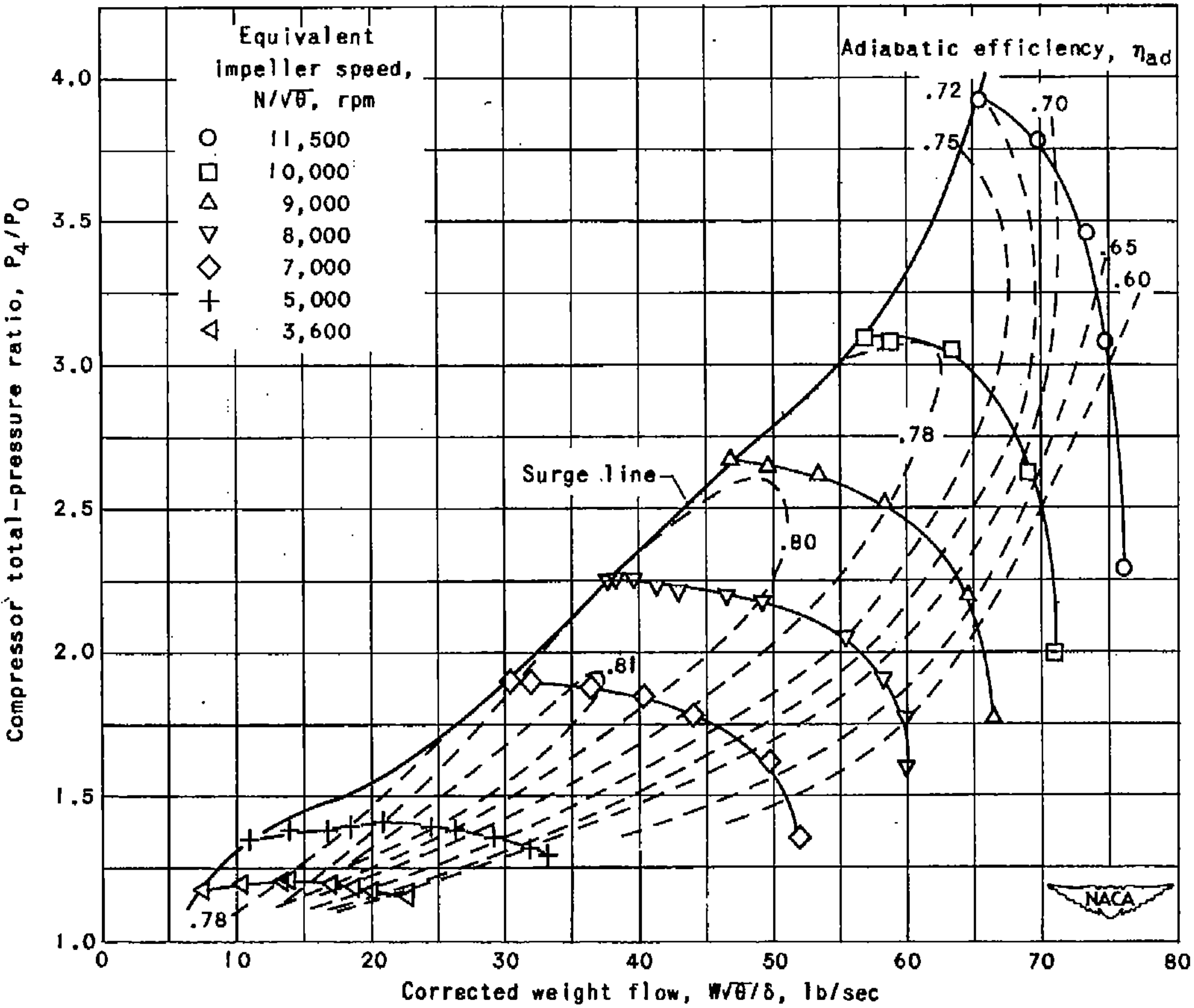

Figure 16. - Performance of revised compressor.

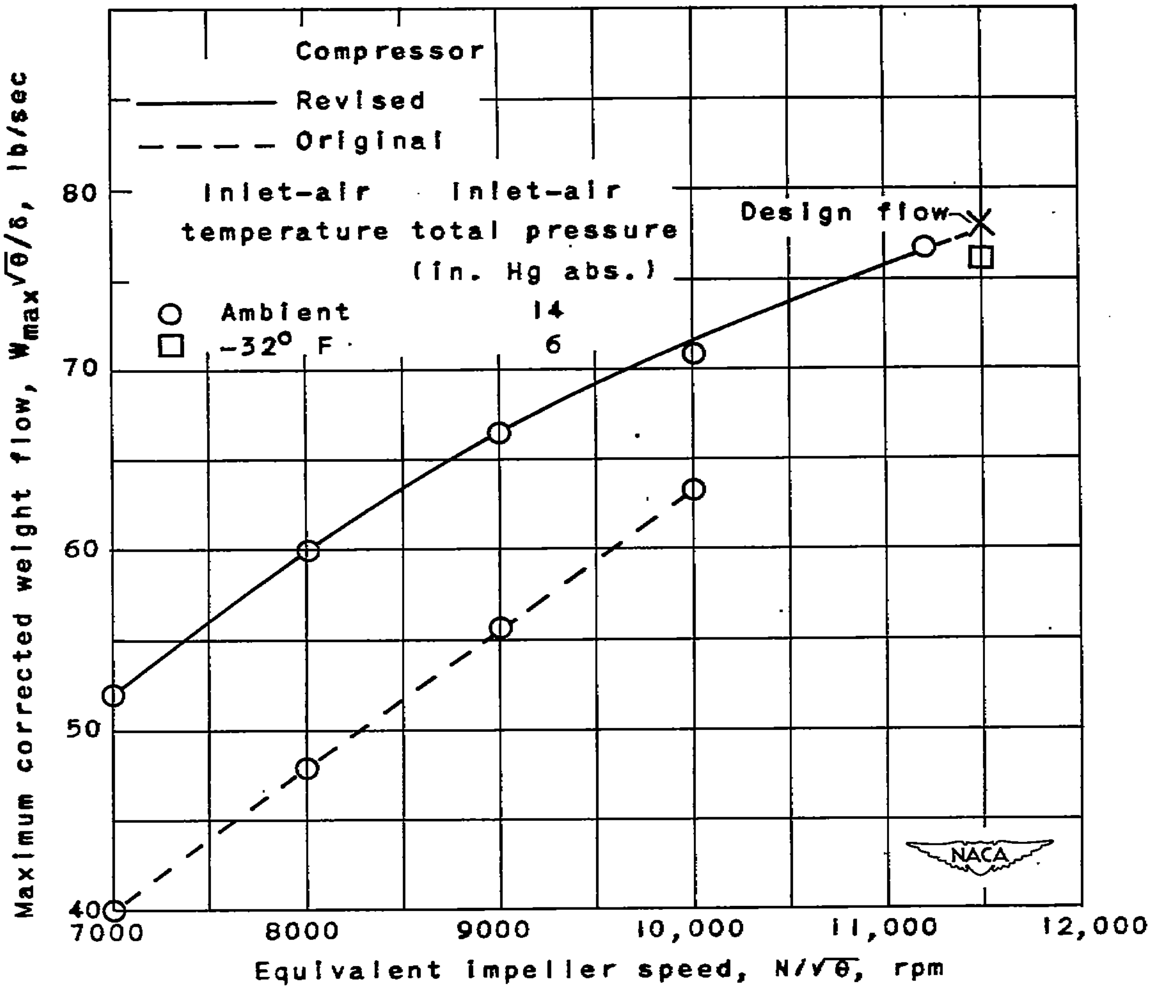

Figure 17. - Effect of compressor revision on maximum corrected weight-flow capacity.

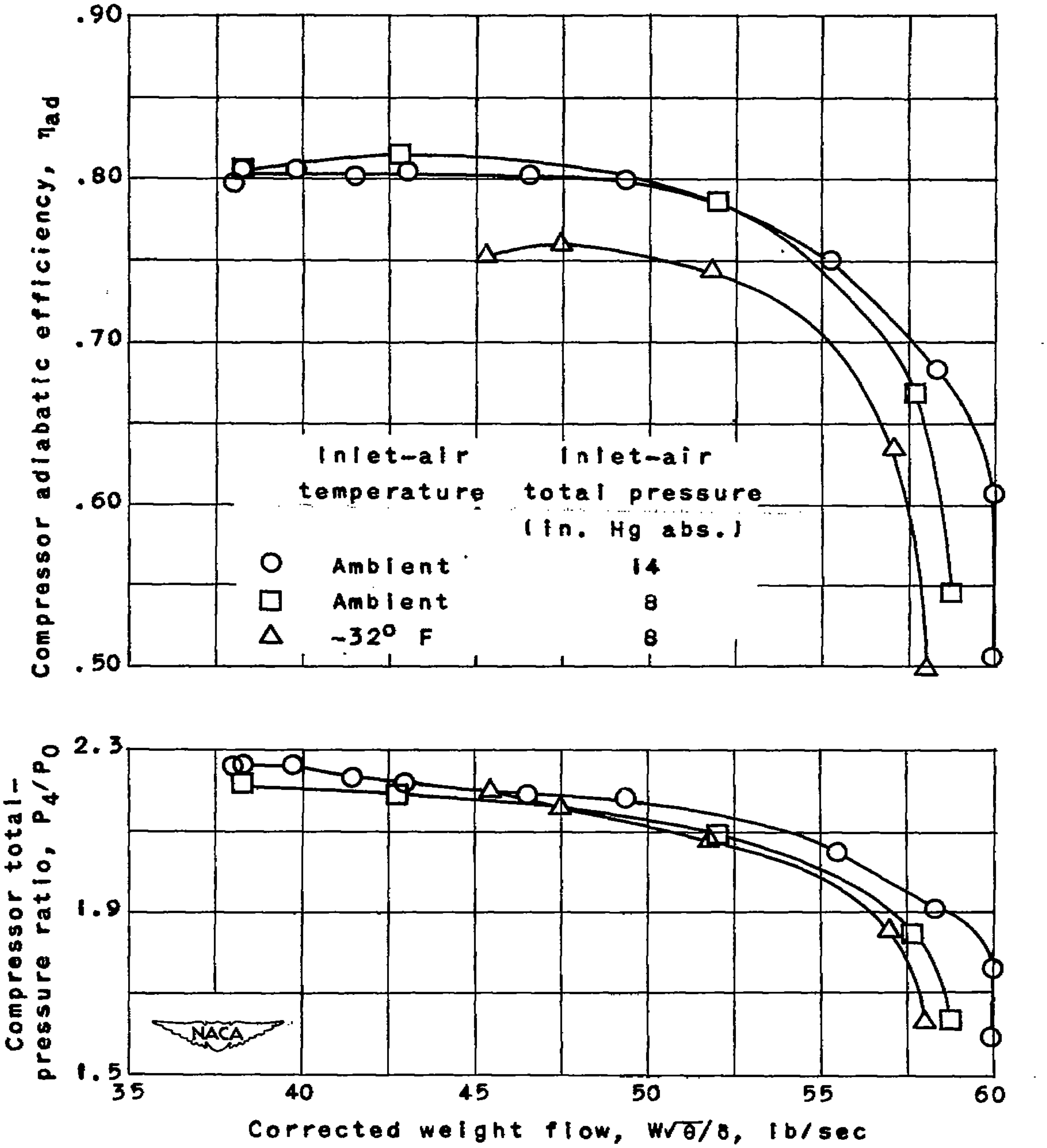

Figure 18. - Effects of varying inlet-air temperature and pressure on compressor performance for equivalent impeller speed of 8000 rpm. Revised compressor.

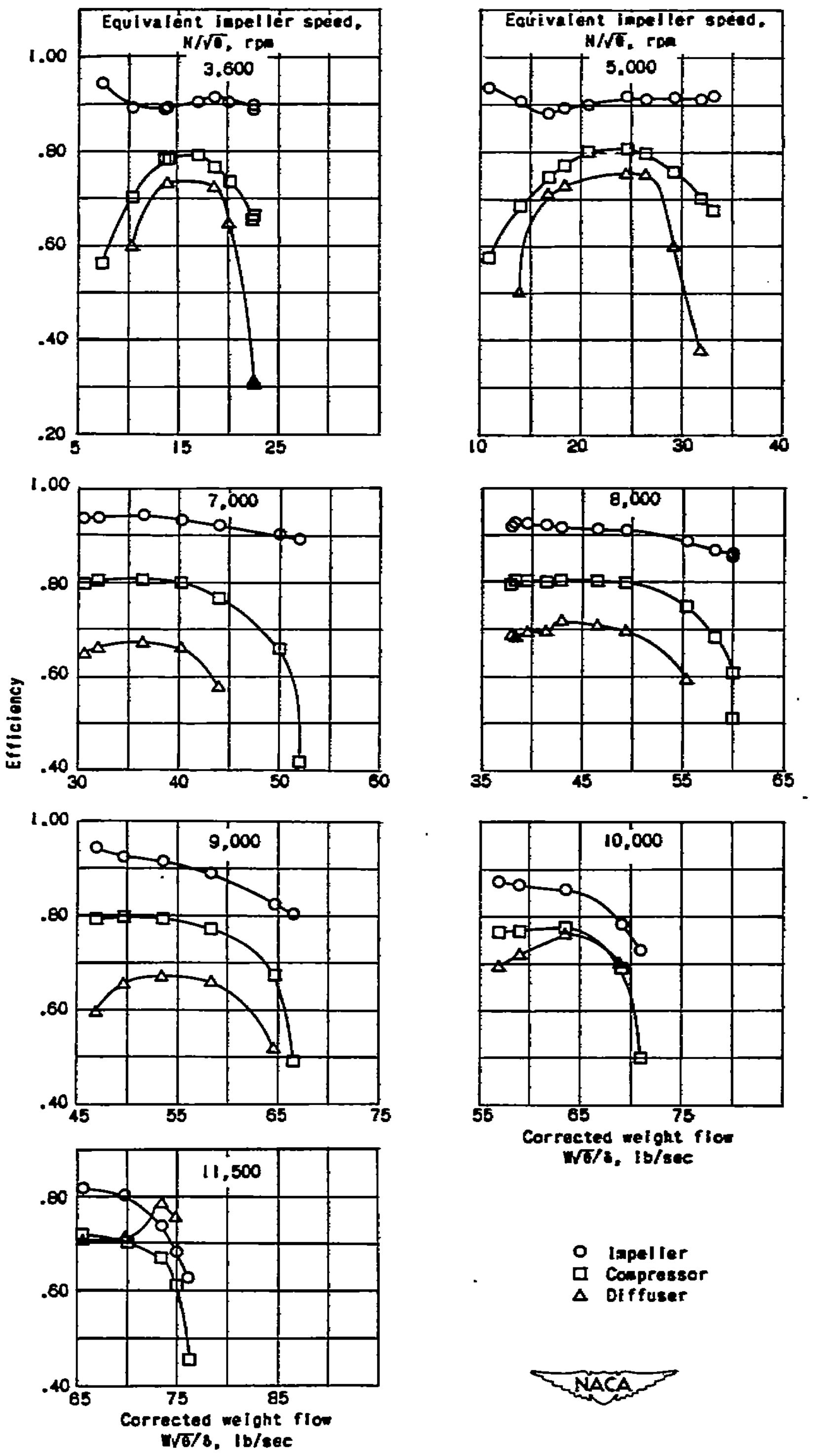

Figure 19. - Performance comparison of compressor, impeller, and diffuser for several impeller speeds. Revised compressor.

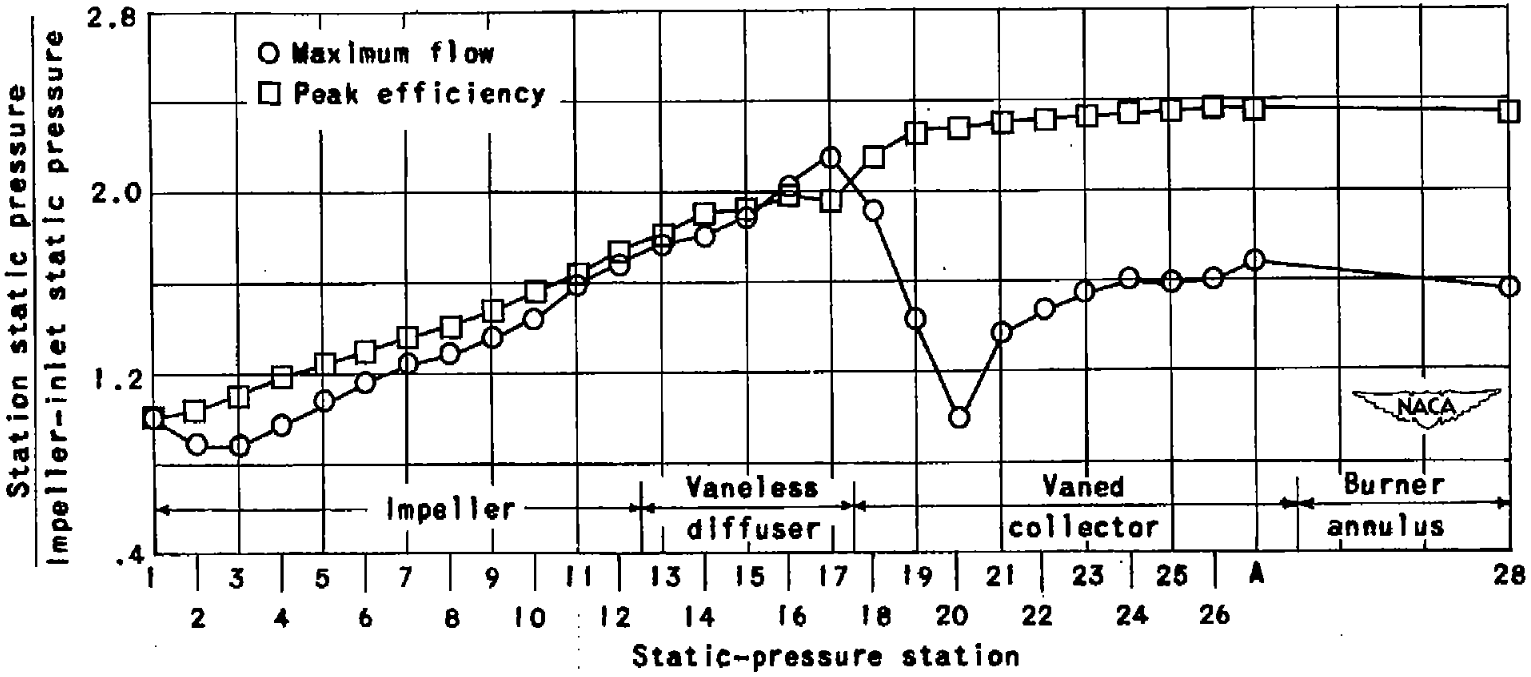

(a) Equivalent impeller speed $N/\sqrt{\theta}$, 8000 rpm.

Figure 20. - Static-pressure variation along compressor flow path. Revised compressor.

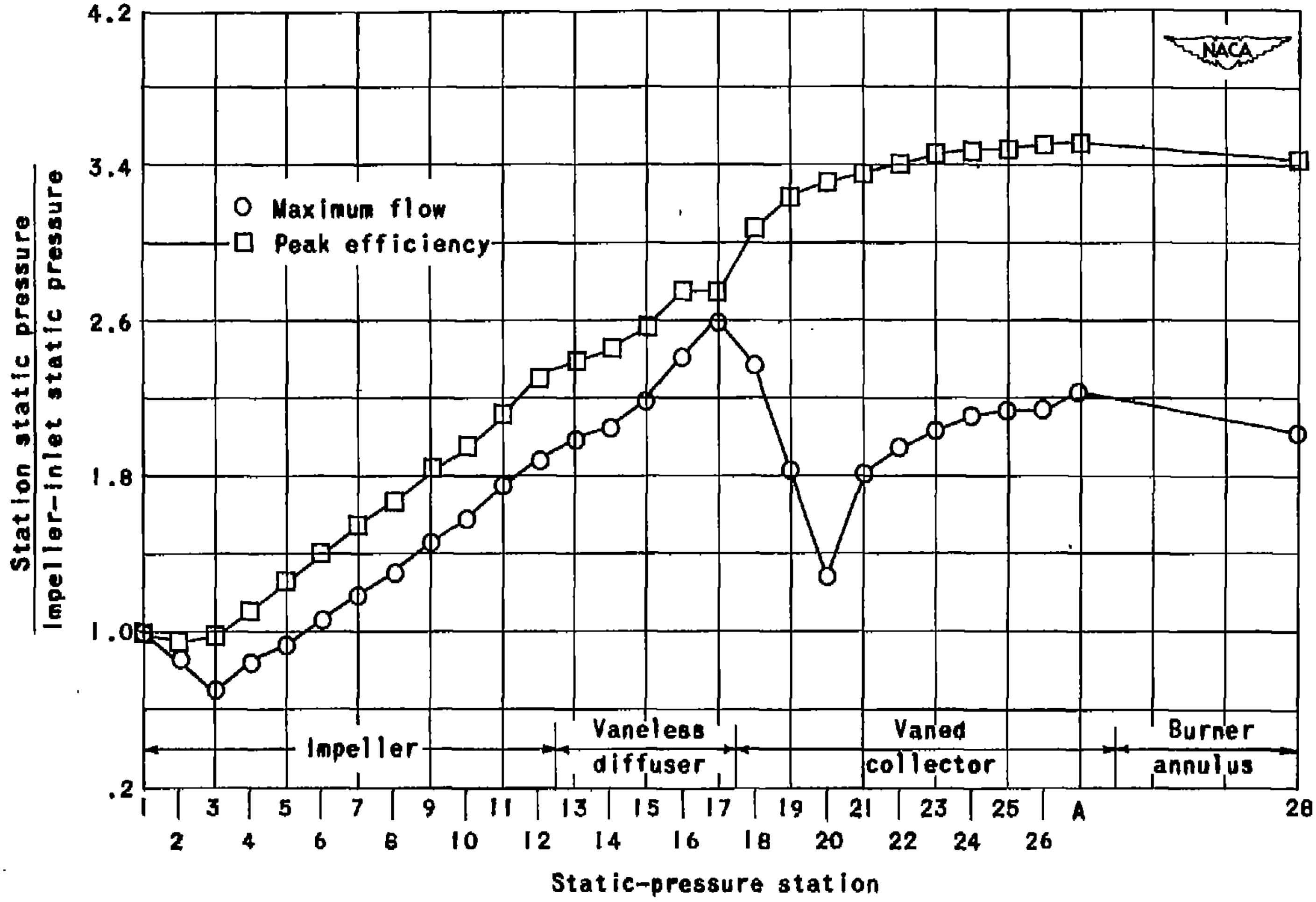

(b) Equivalent impeller speed $N/\sqrt{\theta}$, 10,000 rpm.

Figure 20. - Continued. Static-pressure variation along compressor flow path. Revised compressor.

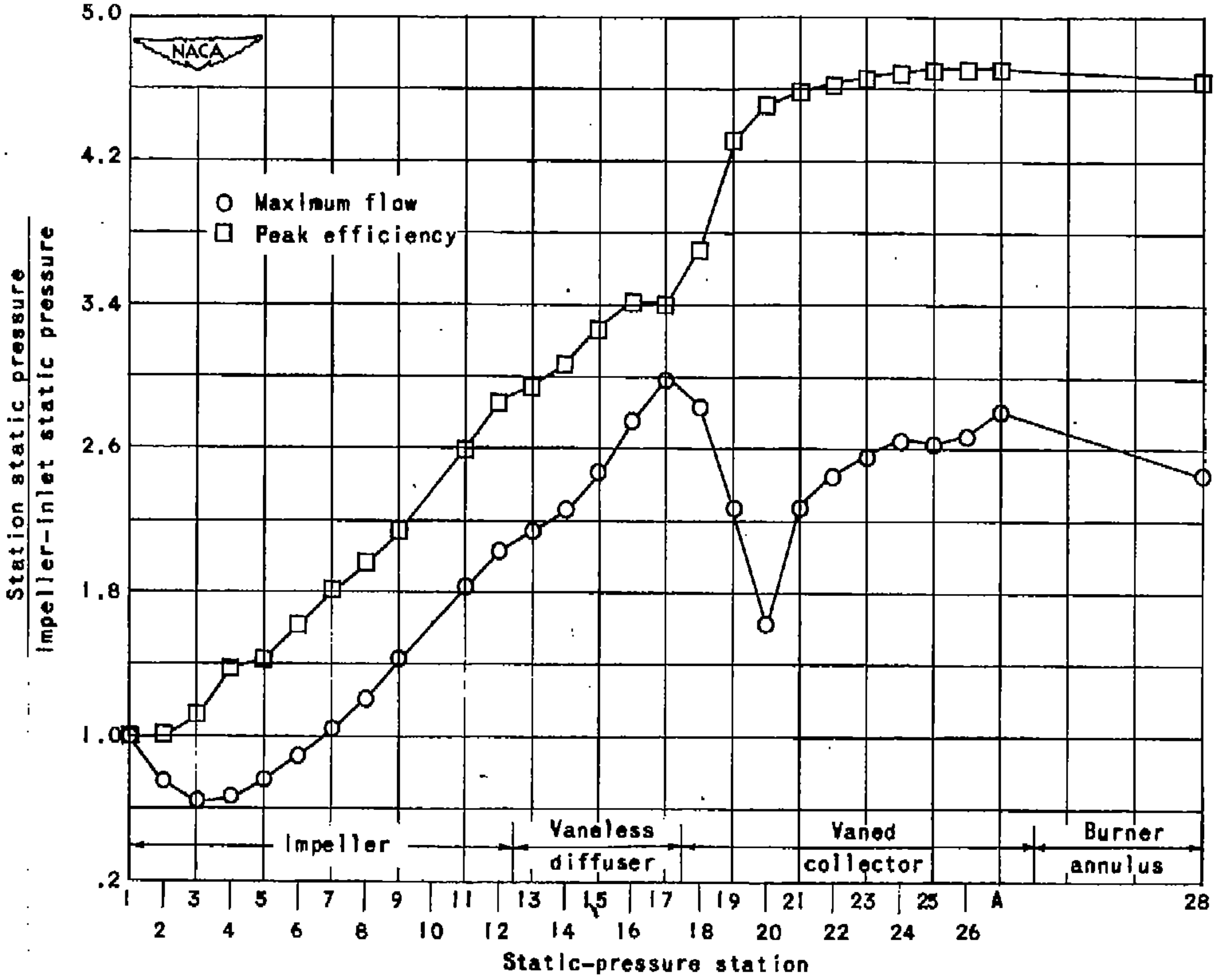

(c) Equivalent impeller speed $N/\sqrt{\theta}$, 11,500 rpm.

Figure 20. - Co[illegible]-pressure variation along compressor flow path. [illegible]vised compressor.

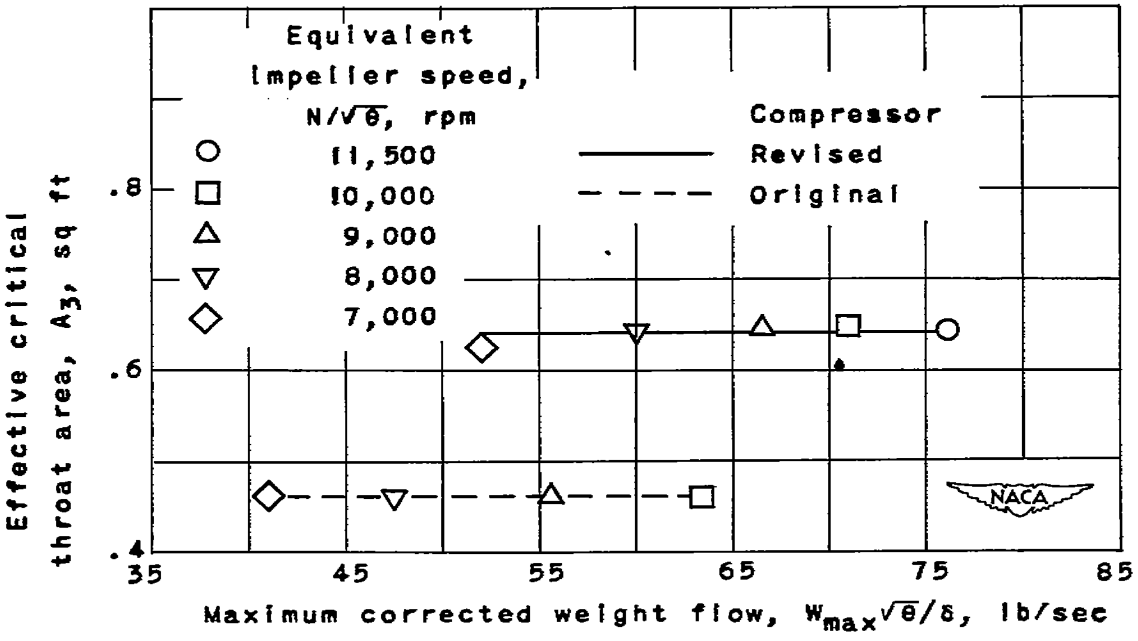

Figure 21. - Variation of effective critical throat area with maximum corrected weight flow for original and revised compressor.

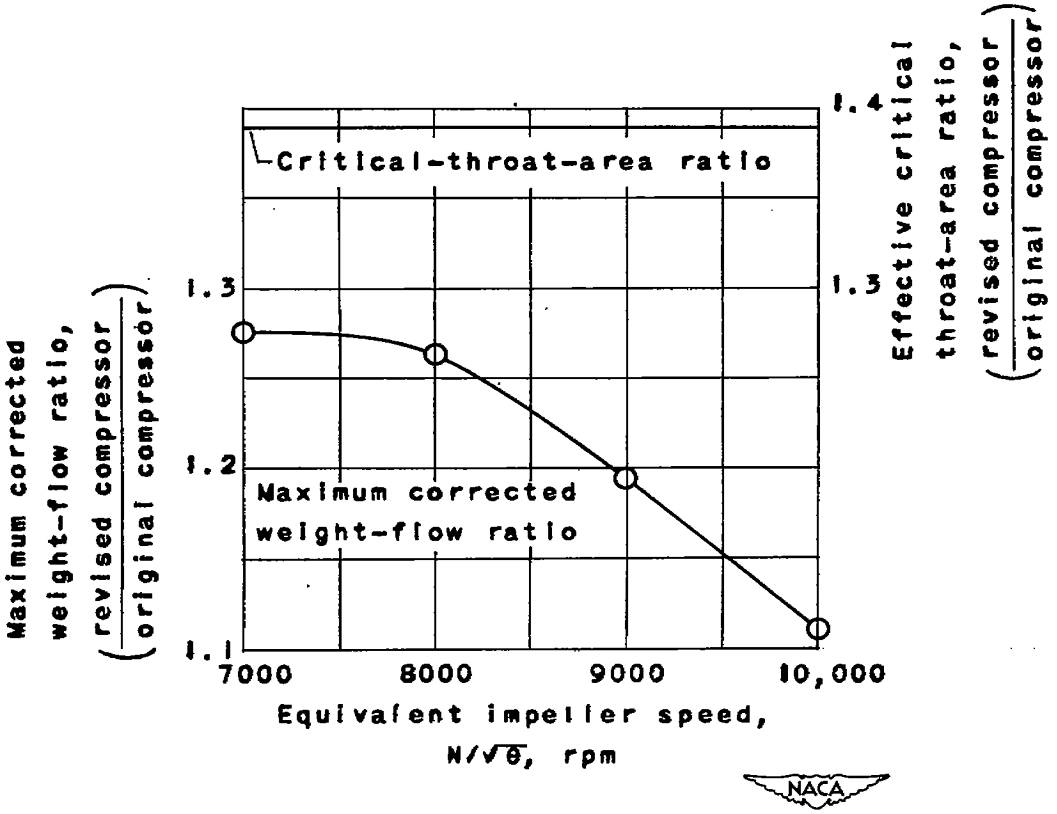

Figure 22. - Comparison of increase in effective critical throat area with increase in maximum corrected weight flow for original and revised compressor.

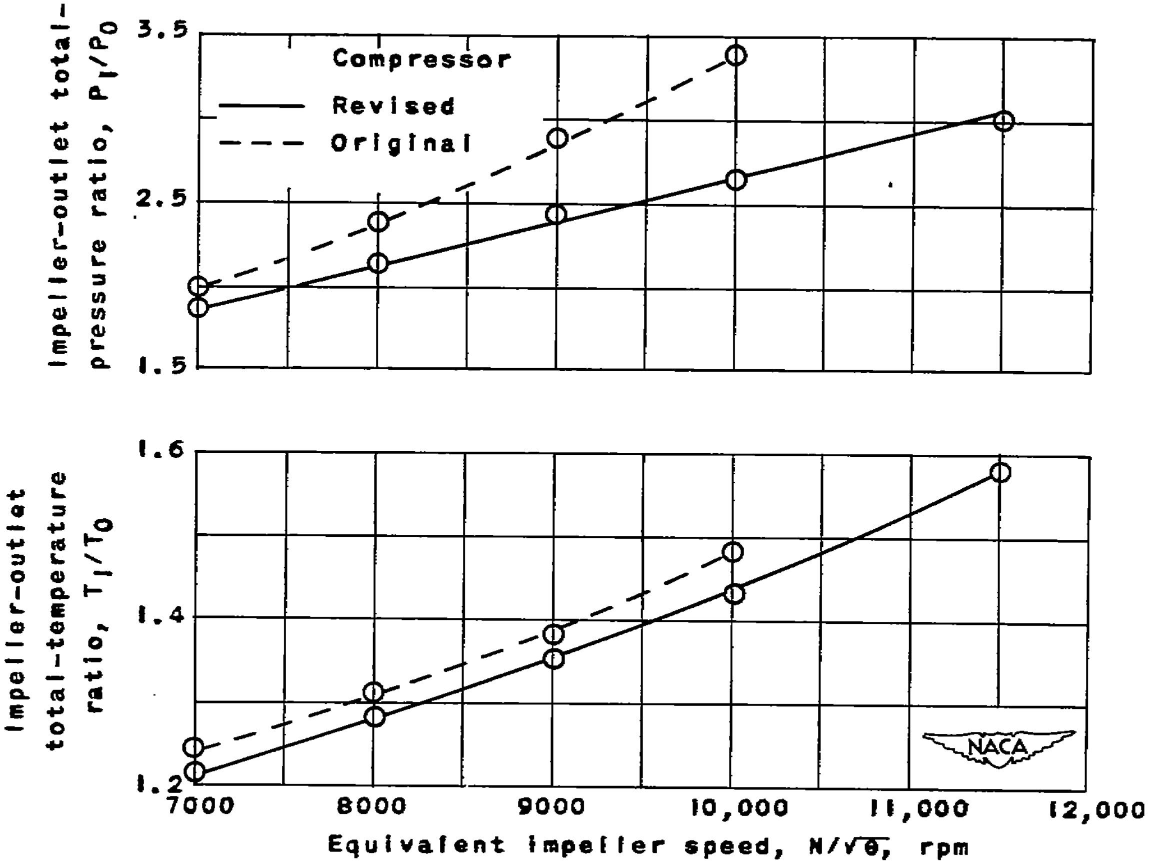

Figure 23. - Comparison of impeller-outlet total-temperature ratio and total-pressure ratio for original and revised compressor at maximum flow.

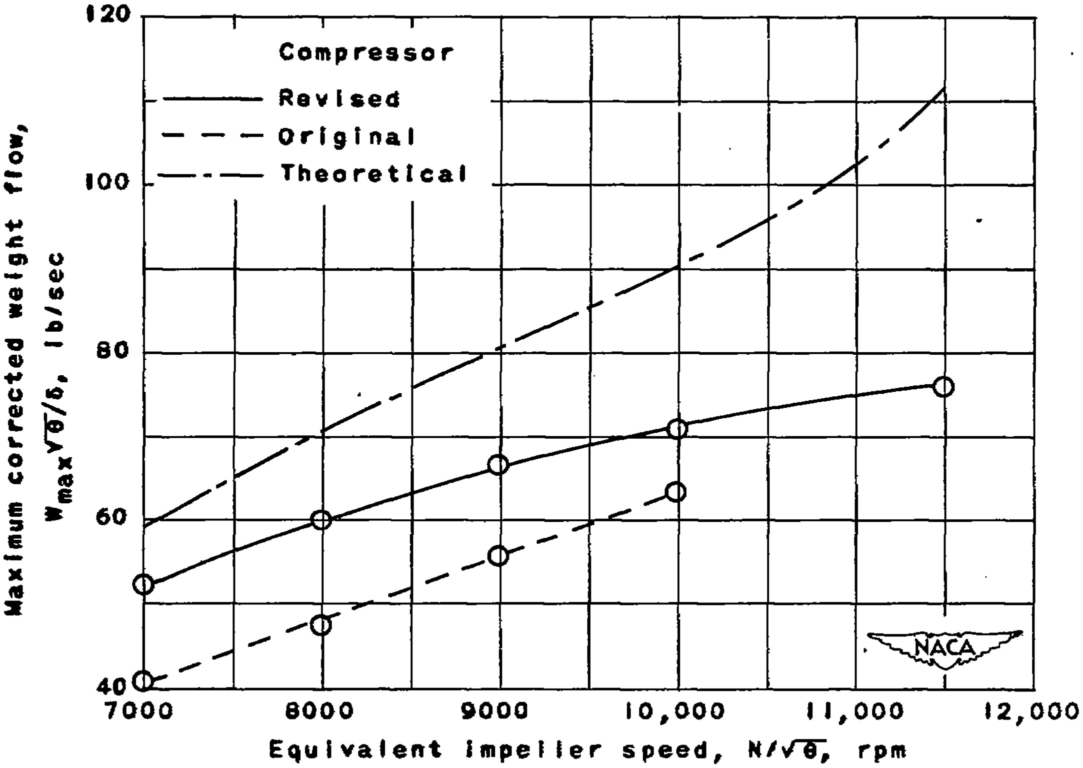

Figure 24. - Comparative values of maximum corrected weight flow for three compressors.

NASA Technical Library
3 1176 01435 5524